Mechanical stress initiates and sustains the morphogenesis of wavy leaf epidermal cells

Amir J Bidhendi[1,2], Bara Altartouri[1], Frédérick P. Gosselin[3], Anja Geitmann[1,2,4,*]

[1]Institut de Recherche en Biologie Végétale, Département de sciences biologiques Université de Montréal, Montreal, Quebec, H1X 2B2, Canada
[2]Department of Plant Science, McGill University, Macdonald Campus, 21111 Lakeshore, Ste-Anne-de-Bellevue, Québec H9X 3V9, Canada
[3]Laboratoire de Mécanique Multi-échelles, Département de génie mécanique, École Polytechnique de Montréal, C.P. 6079, Succ. Centre-ville, Montreal, Quebec, H3C 3A7, Canada
[4]Lead Contact
*Correspondence: geitmann.aes@mcgill.ca

Plant cell shape is governed by the mechanical properties of the cell wall and is intimately related to the specific function of the cell. Pavement cells covering the surface of plant leaves form wavy interlocking patterns in many plants. We use computational mechanics to simulate the morphogenetic process based on experimentally assessed cell shapes, growth dynamics, and cell wall chemistry. The simulations suggest a multistep process underlying the morphogenesis of pavement cells during tissue differentiation. The mechanical shaping process relies on spatially confined, feedback-augmented stiffening of the cell wall in the periclinal walls, an effect that correlates with experimentally observed deposition patterns of cellulose and de-esterified pectin. We provide evidence for mechanical buckling of the pavement cell walls that can robustly initiate patterns and may precede chemical and geometrical anisotropy.

Keywords

Multistep morphogenesis, plant cell mechanics, mechanical feedback, stress and strain, buckling, leaf, epidermis, pavement cell, interlocking, pectin, cellulose, growth, development, cell wall, finite element analysis, fluorescence imaging

Highlights

- A multistep morphogenetic process shapes wavy pavement cells.
- Stress/strain stiffening following the buckling of the cell walls forms a feedback loop shaping wavy pavement cells.
- Mechanical modeling predicts spatial variations in the mechanical properties of leaf epidermal cells.
- Bundled cortical microtubules, cellulose microfibrils, and de-esterified pectin locate in necks of wavy pavement cells.
- Microtubule polarization is preceded by a mechanical anisotropy breaking.

Introduction

Differentiation of plant cells in the apical or lateral meristems begins with simple spherical or polyhedral bodies produced by cell division. The cells formed at the shoot and root apical meristems are approximately cubic whereas those deriving from lateral meristems tend to be longitudinal and brick shaped—all possess a relatively simple geometry. During differentiation of plant organs, tissue-dependent cell types emerge that exhibit a kaleidoscopic array of different morphologies, depending on location and function (Mathur, 2004). In plants, the morphodynamics of differentiating cells is intimately linked to the mechanics of the extracellular matrix—the cell wall. While shaping processes are regulated by the cytoskeleton, they are not mechanically driven by it, since the forces generated by cytoskeletal arrays are too small to act against the wall (Money, 2007). The plant cell wall is a hydraulic structure that regulates the shape of the plant cell by balancing the intrinsic turgor pressure and external mechanical constraints through its compliance. The turgor pressure propelling cell expansion is a scalar acting uniformly on all cellular surfaces. Therefore, to grow into complex shapes, plant cells must meticulously modulate the mechanical properties of the wall in space and time and at subcellular scale. This is important since, unlike animal cells, morphogenetic processes in plant cells are typically irreversible.

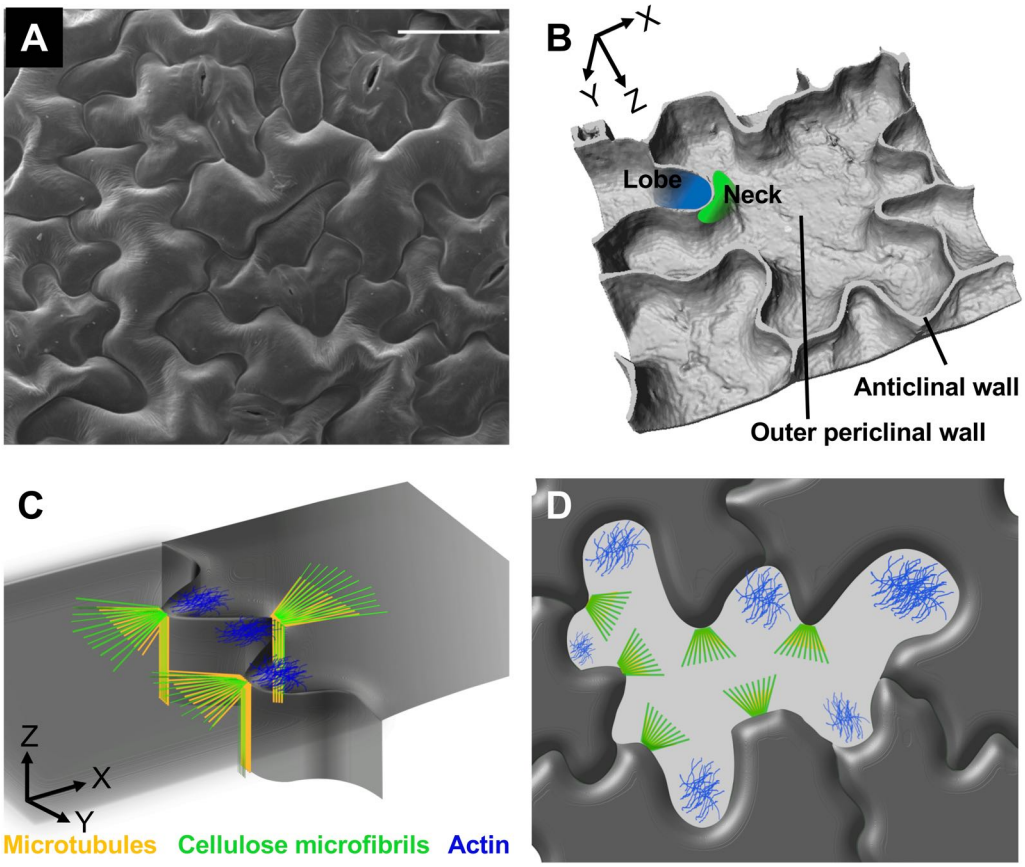

Fig. 1. Pavement cells in the leaf epidermis of *Arabidopsis thaliana*. **A)** Scanning electron micrograph showing jigsaw puzzle shaped pavement cells (Scale bar = 30 μm). **B)** 3D reconstruction of confocal microscope z-stack of a pavement cell consisting of the outer periclinal and anticlinal cell walls. **C)** Local deposition of cellulose microfibrils (red) guided by microtubules (green) on anticlinal and periclinal walls proposed by Panteris and Galatis (2005). Tips of lobes display actin arrays (blue) as shown by (Armour et al., 2015; Fu et al., 2005) **D)** Paradermal view of pavement cells showing localization of microtubules, cellulose microfibrils, and actin microfilaments.

The wall of growing plant cells, the primary wall, is a composite material comprising several types of polysaccharides, proteins, ions and water. Two main structural components of the primary cell wall are pectins and cellulose microfibrils (Bidhendi and Geitmann, 2016; Cosgrove, 2015, 2018). Cellulose microfibrils are generally recognized as the main load-bearing component that confer anisotropy (Anderson et al., 2010; Baskin, 2005; Burgert and Fratzl, 2009; Crowell et al., 2011), whereas pectin chemistry influences the local stiffness of the wall (Bidhendi and Geitmann, 2016; Braybrook and Peaucelle, 2013; Carter et al., 2017; Giannoutsou et al., 2016; Torode et al., 2017). Both cellulose microfibrils and pectins are thought to direct the local shaping of cells, but hitherto these concepts have mostly been investigated in cells with simple shapes such as pollen tubes (Fayant et al., 2010), root hairs (Shaw et al., 2000), trichome branches (Yanagisawa et al., 2015), or cells of root and shoot epidermis (Baskin, 2005; Peaucelle et al., 2015). How growing plant cells form complex shapes is poorly understood (Geitmann and Ortega 2009).

Some of the most intriguing manifestations of plant cell morphogenesis occur at the surface of leaves. The three cell types composing the leaf epidermis—guard cells, trichomes and pavement cells—are geometrically very different from one another. Formation of interlocking protrusions and indents in leaf epidermal cells is a common trait some variation of which can be found as widely spread as in the eudicotyledons, monocotyledons, gymnosperms and ferns (Vofely et al., 2018). The resulting pattern resembles a jigsaw puzzle (Figs. 1A and B). This complex growth pattern of leaf pavement cells makes them an ideal model to study mechanisms underlying the formation of complex shapes in plant cells (Bidhendi and Geitmann, 2018; Jacques et al., 2014; Majda et al., 2017; Mathur, 2004; Sapala et al., 2018; Szymanski, 2014). Various biomechanical concepts have been proposed to explain the formation of lobes in pavement cells (Jacques et al., 2014; Korn, 1976; Korn and Spalding, 1973; Majda et al., 2017; Watson, 1942). Hypotheses range from bending of the cell walls resulting from the growth of cells in a confined space, inhibition of pavement cell expansion due to forces from cuticle or inner mesophyll layers to localized outgrowth of the anticlinal cell walls (Korn, 1976). The 'localized outgrowth' hypothesis is the most widely accepted explanation for shape generation in pavement cells. It states that regions of localized outgrowth penetrate into neighboring cells (Korn, 1976). The orchestrated formation of alternate necks and lobes in adjacent cells implies that a signaling mechanism must exist that operates across the walls connecting neighboring cells. The concept of local growth activities has been correlated with well-organized microtubule bundles in neck regions and accumulation of actin microfilaments at sites of lobes both of which had been proposed to be regulated by auxin-mediated antagonistic pathways (Fu et al., 2005; Fu et al., 2002; Xu et al., 2010), but these notions warrant further investigation (Belteton et al., 2017). Although their exact roles in this context are poorly defined, actin microfilaments and microtubules appear to be instrumental in determining pavement cell shape (Mathur, 2004, 2006; Smith, 2003; Smith and Oppenheimer, 2005; Zhang et al., 2011). Evidence for this has been provided by pharmacological and mutation-mediated interference with cytoskeletal functioning which

affects pavement cell shape (Baskin et al., 2004; Baskin et al., 1994; Mathur, 2004). Actin microfilament patches in lobes are suggested to promote local outgrowth through exocytotic delivery of new wall-building materials and wall-loosening agents such as expansins (Cosgrove, 2005; Fu et al., 2002; Panteris and Galatis, 2005; Smith, 2003). Microtubules are generally thought to regulate plant cell wall mechanics by determining the orientation of newly deposited cellulose microfibrils (Crowell et al., 2009; Gu et al., 2010). This is accomplished by guiding the location of insertion and trajectory of cellulose synthase (CESA) enzymes at the surface of the plasma membrane (Hamant and Traas, 2010). Cellulose microfibrils are therefore thought to mimic the orientation of microtubules and, inversely, microtubules have been used as a proxy to infer the localization of cellulose microfibrils (Eng and Sampathkumar, 2018; Fu et al., 2005; Zhang et al., 2011). In pavement cells, two effective microtubule arrays are suggested to be involved in the formation of a neck region and add cellulose microfibrils at these locations. In an influential paper, Panteris and Galatis (2005) proposed that a cortical array is associated with the anticlinal wall of a neck and is contiguous with a cortical array extending under the periclinal wall of the same neck (Fig. 1C and D). Actin filaments are suggested to be present mostly in lobe regions promoting expansion (Panteris and Galatis, 2005) (Figs. 1C and D). Panteris and Galatis proposed that the essence of shape formation in pavement cells involves a distinct cellulose configuration on the neck side of the undulations and a resulting stiffening of the cell wall, but mechanical validation of this concept is elusive (Jacques et al., 2014). The role of the wall polysaccharides in mediating the mechanical conditions has not been investigated in detail. Further, cellulose orientation has not been directly visualized in pavement cells using fluorescence techniques. In a recent study by Sampathkumar et al. (2014), the effect of pavement cell shape on the stress state of the cell wall and microtubule reorganization was modeled mechanically. However, while this relationship may constitute one step of a patterning mechanism governing development, it does not explain the initiation of polarized shapes and lobe formation *de novo* (Sampathkumar et al., 2014). Importantly, however, in this study a convincing causal link is made from cell shape to spatial orientation of microtubules, but the reverse question of the effect of microtubule orientation (or of cellulose microfibrils) on shape development remains unexplored. Recently, Majda et al. (2017) proposed a role for heterogeneous stiffness distribution in the anticlinal walls in formation of border waviness in pavement cells, a 2D morphogenetic concept that we assessed in detail (Bidhendi and Geitmann, 2019). We showed that exclusive focus on the anticlinal wall results in mechanical outcomes that are incompatible with the physiological principles governing pavement cell morphogenesis.

Here, we developed 2D and 3D finite element (FE) models to explore pavement cell mechanics and elucidate how undulating patterns initiate and how they progress starting from simple polygonal geometries. We experimentally validated the predictions made by the simulation by monitoring the spatial distribution of putative mechanical agents including pectin, cellulose microfibrils, and microtubules to assess their predicted behavior in cell morphogenesis.

Results

Verifiable predictions on cell wall deformation through finite element modeling

Finite element modeling was used to simulate the deformation of the cell wall under the effect of internal pressure (turgor) as the deforming force. The finite element method is a mathematical tool widely used in structural mechanics and allows for solving problems involving complex material behaviors and geometries. The results of the mechanical model were used to interpret the experimentally acquired data on cell wall composition and microtubule arrangement to identify the mechano-structural requirements for the formation of interdigitations in pavement cells. Details about the parameters used in models are referenced to and explained in the Supplemental Information where applicable. The undulations in epidermal pavement cells as seen from above correspond to the edge forming the junction between the anticlinal and periclinal walls. We term these undulating edges the *superficial cell borders* (*superficial outer* or *inner* corresponding to outer and inner periclinal walls of a cell, respectively). Since the undulations in the superficial borders of leaf pavement cells correspond to bends in the anticlinal wall, the putative differential expansion of this wall structure has been the primary focus of various experimental or modeling studies (for instance refer to Jacques et al., 2014; Majda et al., 2017). Therefore, we start our modeling approach focusing on anticlinal wall behavior and subsequently move toward more complete descriptions of pavement cell geometry and mechanics.

Generating cellular protrusions based on anticlinal wall modification requires differential turgor pressure

To determine which mechanical conditions would be required to generate a bend in the anticlinal wall resulting in the protrusion of one cell into the neighboring cell, we isolated the problem and developed a finite element model of a section of anticlinal wall between two adjacent cells (Fig. 2A). For this isolated approach, periclinal walls were neglected. The anticlinal wall was constructed to consist of two layers (the primary walls of the two adjacent cells) that are glued together (by the middle lamella, a pectin-rich, thin layer that connects cells in a plant tissue).

The first hypothesis we tested assumes that the curvature in the anticlinal wall is generated because of different growth rates of the two layers, similar to a temperature controlled actuator consisting of two layers with different thermal expansion properties or in curling of thin bilayers (Pezzulla et al., 2016) (Fig. 2A). Relative displacement between the layers is not allowed to mimic the role of the middle lamella. One layer is set to expand at a higher rate by assigning a higher coefficient of thermal expansion—our modeling equivalent of the expansion of cell wall material through the addition of softer material. The simulations show that the layer at the convex (neck) side of the forming bend is the one with the higher rate of expansion (Fig. 2B). However, this contradicts our understanding of the biology of pavement cells. The neck side is thought to be stiffened by microfibrils, whereas an

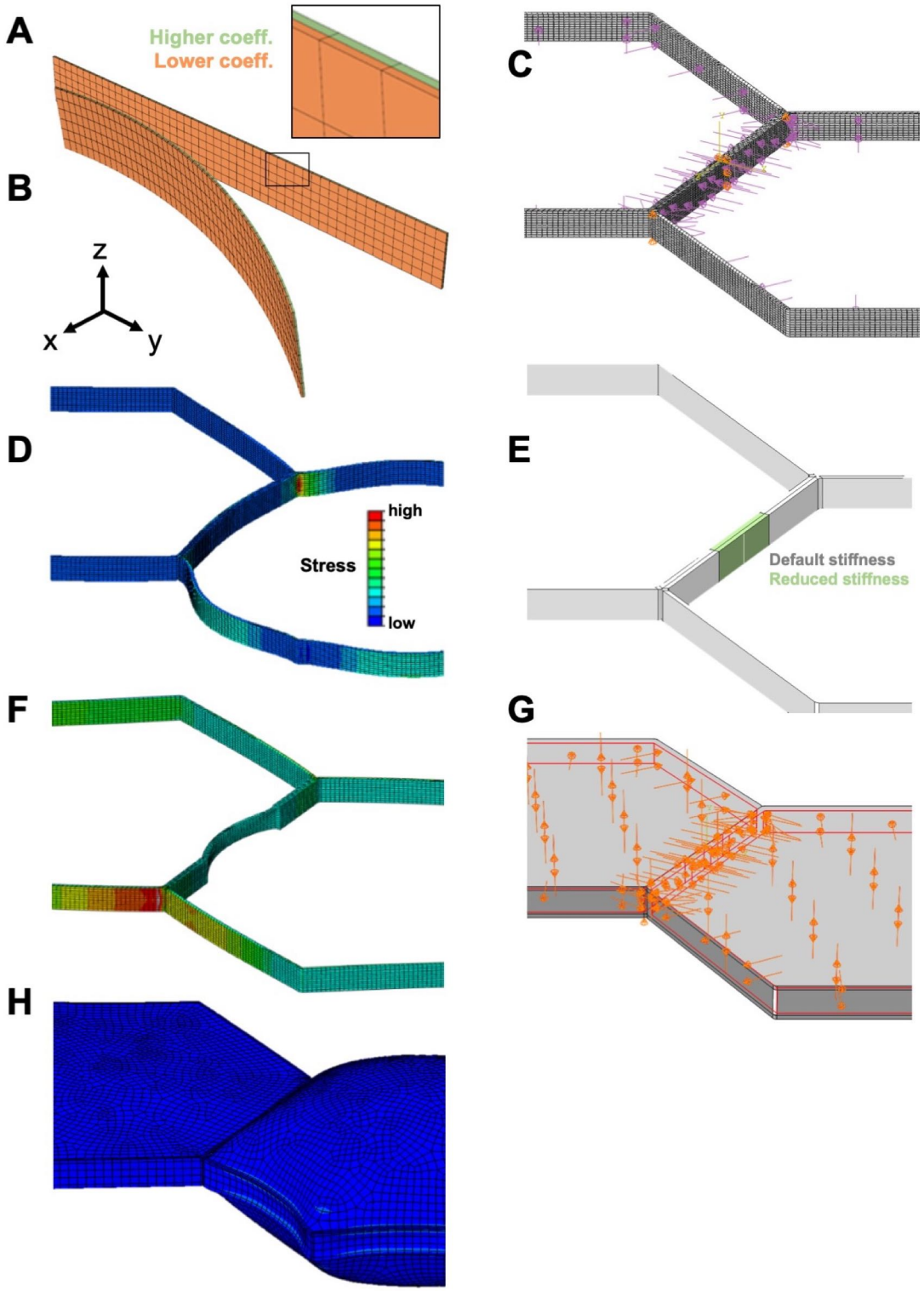

Fig. 2. Finite element model simulating the differential growth of anticlinal cell wall layers. **A)** Representation of anticlinal wall separating adjacent cells by two material layers glued together at their interface. One layer (green) is given a higher coefficient of thermal expansion to simulate higher growth rate; the right end of the wall may move in space. **B)** Differential expansion of the layers results in the formation of a curvature with the faster-expanding layer forming a convex curve. **C)** Finite element model of the walls of two adjacent cells. Only anticlinal walls are considered; loads are applied on internal surfaces of the walls. **D)** In the presence of differential pressures and uniform anticlinal wall stiffness the anticlinal wall forms a second order curve into the cell with lower pressure. Heatmap represents stress. **E)** A spatially confined region (green) in the anticlinal wall is assigned a softer value than the default stiffness (gray). **F)** A turgor differential results in the formation of a local protrusion into the cell with lower turgor. **G)** Periclinal walls are added to the model. **H)** When periclinal walls have isotropic material properties, the cell with the higher turgor pressure forms a more pronounced swelling in z direction pulling the anticlinal walls inwards.

actin array at the concave side of undulations (Fig. 1D) suggests that delivery of new matrix material by exocytosis occurs predominantly on the lobe side (Panteris and Galatis, 2005). The finite element model based on asymmetric anticlinal wall expansion, therefore, seems unable to provide a description of wave formation that is consistent with the known biological processes.

The second hypothesis we tested is not based on modulation of wall growth behavior, but on that of the acting forces. We examined whether differential turgor in neighboring cells can generate a bend in the anticlinal wall. For modeling purposes, the cell geometry is hexagonal (Figs. 2C and S1A). As above, non-slipping non-separable contact is considered between the anticlinal wall layers in contact. This is to reflect the adhesion between the cell wall layers at the middle lamella. Turgor pressure is exerted on the internal surfaces of both cells, and the model allows for independent adjustment of the turgor pressure in each cell. At equal turgor pressures in the two neighboring cells, the overall shape and the relative position of the midline of the anticlinal wall in contact between two cells does not change as the forces acting on the two sides cancel each other out. If differential turgor

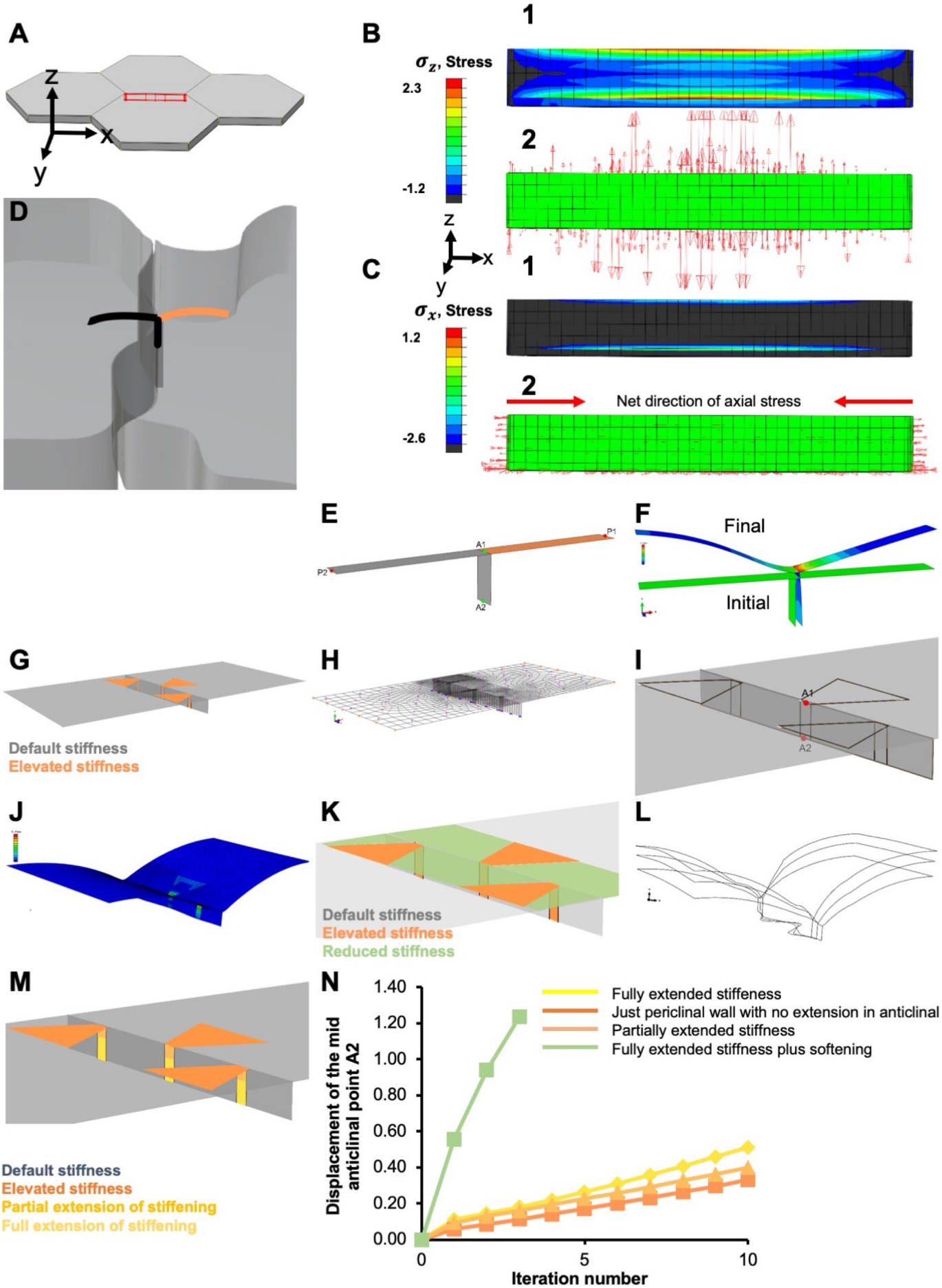
A
z
x
y
B
1
σ_z, Stress
2.3
-1.2
2
C
1
σ_x, Stress
1.2
-2.6
2
Net direction of axial stress
D
E
P1
A1
P2
A2
F
Final
Initial
G
Default stiffness
Elevated stiffness
H
I
A1
A2
J
K
Default stiffness
Elevated stiffness
Reduced stiffness
L
M
Default stiffness
Elevated stiffness
Partial extension of stiffening
Full extension of stiffening
N
Fully extended stiffeness
Just periclinal wall with no extension in anticlinal
Partially extended stiffness
Fully extended stiffness plus softening
Displacement of the mid anticlinal point A2
1.40
1.20
1.00
0.80
0.60
0.40
0.20
0.00
0
5
10
Iteration number

Fig. 3. Finite element simulation of stresses and resulting deformations upon load application through turgor pressure. **A)** Multicell finite element model used to assess stress pattern in the anticlinal walls between hexagonal cells. The red square marks the anticlinal wall that is shown isolated in B and C to reveal stresses. In this wall, stress components in vertical direction **(B)** are significantly larger than in horizontal direction **(C)**. **B-1)** Color-coded distribution of vertical (Z direction) component of wall stress. **B-2)** The arrows indicate the magnitude and direction of the vertical stress. **C-1)** Color-coded distribution of axial (X direction) component of wall stress. **C-2)** The arrows indicating axial stress in horizontal direction show the compressive stresses resulting from the vertical expansion. Stress values are relative as normalized input values are used in models (see modeling procedures and Supplemental Information). **D)** Position of segment crossing two adjacent cells modeled in **E-N**. Segment comprising sections of the periclinal walls of the two adjacent cells and the shared anticlinal wall. **E)** Shell model of wall segments. Pressure load is applied on lower surface of the periclinal walls, similar to loading in 2D beam model shown in Fig. S2A. **F)** Deformation in the shell model is similar to the beam model. **G)** Finite element model with alternate placement of stiffened regions on the periclinal and anticlinal walls of two adjacent cells. **H)** Turgor pressure is applied to inner surface of the periclinal walls (no pressure on the anticlinal wall as the acting forces cancel each other out). **I)** Position of fiducial markers used to monitor shape formation by measuring the displacement of the anticlinal wall. **J)** Initiation of undulations in the first iteration of the model. Heatmap represents von Mises stress. **K)** Finite element model with alternate placement of stiffened regions on the periclinal and anticlinal walls of two adjacent cells with cell wall softening in areas between the incipient necks. **L)** Evolution of undulations for three iterative load applications. **M)** Stiffening extensions on the anticlinal wall extending into different depths. **N)** Displacement of the anticlinal wall mid-point (A2) under different wall stiffening-softening scenarios reveals that fully extended stiffening leads to more pronounced undulation, but the effect is small compared to that of a softening in the periclinal wall. The stiff, soft and default regions were assigned Neo-Hookean elastic constants (C_{10}) of 10, 0.05 and 0.5, respectively.

pressures are applied, the cell with the higher pressure curves into the cell with lower pressure (Fig. 2D). A more spatially confined deformation similar to a lobe protrusion can be achieved if the anticlinal wall layers are made softer on a limited length, combined with the application of differential pressure (Figs. 2E and F). To produce a local protrusion, this locally reduced stiffness must be applied to both wall layers in the same region (although not necessarily at the same magnitude). If only one wall layer is softened, the deformation resulting from the differential pressure application causes an overall bend of the entire wall section rather than a spatially confined protrusion.

Mechanical changes confined to anticlinal walls cannot reproduce cell growth

To investigate whether the predictions made by the isolated anticlinal wall model remain valid in the presence of the periclinal walls, these are added to the finite element model (Figs. 2G and H). The aspect ratios for cell wall dimensions are adopted from typical values obtained from pavement cells in *Arabidopsis* cotyledons at early stages of development (e.g., Fig. S5G). Periclinal wall thickness is set to be identical to that of the anticlinal walls, and the material is configured to be isotropic with uniform stiffness. The pressure in the right cell is set 10:1 compared to the cell on the left. The simulations show that upon application of the turgor pressure, the cells swell out of the plane, the free anticlinal walls displace inward, reducing the in-plane cell surface (Fig. 2H). The anticlinal wall shared with the neighboring cell displaces toward the cell with higher pressure (Figs. S1B and S1D). Softening of the whole anticlinal wall in the contact region between the cells results mainly in an upward stretch of this wall, a displacement toward the cell with a higher pressure with a bulge in the mid-depth of the anticlinal walls toward the cell with lower pressure. However, the superficial borders of the anticlinal and periclinal walls remain relatively straight (Fig. S1C). A high ratio of turgor pressures (100:1) was used to produce a discernible behavioral trend. Even at this unphysiologically high pressure differential, the protrusion remains isolated to the anticlinal wall and forms no visible wave at the superficial borders of the cells. It should be noted that in the biological system, even relatively small turgor differentials between adjacent cells may be difficult to achieve or maintain due to the existence of intercellular channels, plasmodesmata, which allow for a certain degree of fluid exchange. Similar results are obtained when the softening is confined to an isolated region of the contact anticlinal wall. Therefore, unlike the isolated anticlinal wall model, if cell walls are isotropic, pressurization of a cell does not generate behavior expected from a differentiating epidermal cell. It neither increases the area of the cell in plane nor does it generate anticlinal curvatures into the adjacent cells. These results can be explained considering the respective surface areas of the periclinal and anticlinal walls. Since the combined inner and outer periclinal walls of a typical epidermal cell possess a higher surface area compared to the combined anticlinal walls of the same cell (see for instance Fig. S5G), the force of the turgor pressure acting upon them ($F = P \times A$, where P is the pressure and A is the surface area on which the pressure is exerted) is greater and results in a net out-of-plane deformation of the cell. This is not to consider that, regardless of the difference in surface area, the effect of turgor pressure on anticlinal walls can be cancelled out when the pressure inside neighboring cells are equal. The resulting deformation of the periclinal walls leads to a contraction of the in-plane dimensions of the cell. These simulations therefore suggest that isotropic softening of the anticlinal walls does not cause epidermal plant cells to grow in plane.

An important consequence of the presence of the periclinal walls is the tensile force that is exerted on the anticlinal walls through the pressure that causes the periclinal wall to bulge out of the epidermal plane. To assess the resulting stresses generated in the anticlinal wall, the FE model was extended to represent four cells (Fig. 3A). The pressure is set equal in all cells. The anticlinal wall to be analyzed is the one in the center between the four cells. Boundary conditions are applied to the corners of the lower periclinal walls to simulate an attachment to the underlying mesophyll layer. In the anticlinal walls, the vertical component of the stress was considerably larger (σ_z against σ_x, Figs. 3B and C), constituting the net direction of stress in these walls. In other words, finite element modeling indicates that mean stress direction caused by turgor in the anticlinal wall of a pavement cell is in direction perpendicular to the plane of leaf. Further, consistent with the results mentioned above, the results indicate that the transverse component of the stress (σ_x) can become locally negative (compressive). As compressive

forces have the potential to cause buckling, these findings indicate that buckling in the anticlinal walls can arise simply from cell geometry and turgor load.

Differential stiffness in the periclinal wall can generate cell border undulations

Given that spatial variations in the mechanical properties of anticlinal walls cannot yield wall undulations similar to those seen in pavement cells, we hypothesize that considering the mechanical properties of periclinal walls might be crucial in growth and shaping of cells. We postulate that to form undulating borders, the mechanical properties of the periclinal wall must vary in alternatingly arranged, spatially confined regions as initially proposed by (Panteris and Galatis, 2005) (Fig. 1C). We first consider the generation of an isolated bend in the cell border by focusing on a transverse segment including both anticlinal and periclinal wall segments. In this one-dimensional approach, the periclinal walls of two adjacent cells are modeled with beam elements with a shared anticlinal wall as a vertical beam (Fig. 3D). The periclinal walls of the two adjacent cells are assigned different initial stiffness values, and then turgor pressure is applied to the beam elements (Fig. S2A). The boundary conditions imposed on this model, as with the 2D shell model of Fig. 3E, enable horizontal (in x direction) movement for the end-point of the anticlinal wall (A2) which represents the midway point of the entire anticlinal wall depth. The periclinal end-points (P1 and P2) can only move in the Y direction. The point corresponding to the connection of the anticlinal wall with the periclinal walls (A1) may move in all directions. Similar boundary conditions are applied to all models henceforth. The 2D thin shell model of the same situation yields the same results confirming the robustness of the predictions independently of the modeling tools (Figs. 3E, F, and S2D). The simulations show that upon application of equal pressure in both cells, the periclinal walls bulge out (in the Z direction), but the wall with the higher stiffness deforms less than the periclinal wall of the neighboring cell. Consequently, the anticlinal wall moves from the mid-point towards the cell with the stiffer periclinal wall. This displacement of the mid-point connecting the two cells could be considered to represent the formation of a protrusion with the lobe being formed by the cell with the lower periclinal wall stiffness (Fig. S2B).

In these simulations, the stiffness differential is implemented *ab initio*; prior to application of the turgor pressure (*ab initio* stiffening). To assess whether the order of the events affects the final state of cell wall deformation, stiffening is implemented in cells already under turgor pressure (*cum tempore* stiffening). Simulations reveal that it does not matter for the outcome whether the cells are under turgor or relaxed when the stiffening of one of the periclinal cell walls is implemented (Figs. S2C-F). In a biological sense, this means that when a segment of the periclinal wall is reinforced, either by deposition of cellulose or by changes in other cell wall polysaccharides, a shift of the relative position of the anticlinal wall toward the cell with the stiffened periclinal wall can be expected upon the next step in development. This does not depend on whether or not the cell wall is under stress when the stiffening occurs.

Differential turgor does not steer pavement cell morphogenesis in the presence of a stiffness differential in the periclinal wall

To verify the influence of turgor pressure on the formation of necks, differential turgor is applied to the two neighboring cells as detailed in the previous section. The results show that in all cases, regardless of the relative turgor pressures in the two cells, the anticlinal wall is displaced toward the cell with the stiffer periclinal wall (Figs. S3A-F) as it stretches less under tension compared to the softer side. In extreme conditions, when the pressure on the stiffened side approaches zero, the horizontal (in x direction) displacement of the anticlinal wall becomes negligible (Figs. S3E and F). This means that the mechanical and geometrical properties of the cell wall are so dominant that they seem to largely override the effect of pressure differentials.

Further, it is observed that when the anticlinal wall is stiffer than the default value (i.e., the value of the non-stiffened periclinal wall), the displacement of mid-points corresponding to points A1 and A2 in Fig. 3E is enhanced as the anticlinal wall deforms less under the effect of the turgor differential (Figs. S3A-F). Taken together, the simulations suggest that differential turgor pressure is not a requirement to form pavement cell undulations, but that cell wall mechanics seems to be dominant.

The relation between stiffness differential and undulation is non-linear

To assess how different the stiffnesses between the lobe and neck on the opposing periclinal walls must be for an undulation to evolve, different ratios of stiffness between the stiffened and default periclinal walls are examined by monitoring the resultant displacement of the anticlinal wall. As the ratio increases from 1 to 5, the displacement of the anticlinal wall increases rapidly, but beyond this value the deformation plateaus (Fig. S4A). At this point, the stiffer side behaves as a rigid structure compared to the softer (lobe) side. Unless turgor pressure is increased, any additional stiffness in the stiffer wall does not result in a perceivable increase in horizontal (in x direction) displacement of the anticlinal wall.

We then wanted to test whether subtle stiffness differentials would lead to undulations if load application is applied repeatedly. Iterative load application is accomplished by re-zeroing the stress developed in shell elements following each load application and by repeating the simulation, starting off with the last deformed shape. Running the simulation for 3 iterations shows that the resulting horizontal (in x direction) displacement of the anticlinal wall is negligible compared to the vertical (out of epidermis plane, in the Z direction) deformation (Fig. S4B). Therefore, when continued, the cells only balloon out of the plane, not forming discernable undulations. This demonstrates that repeated load application does not cause more pronounced wave formation if the stiffness difference is negligible to begin with, and remains constant. A sufficiently large stiffness ratio between the two periclinal wall segments is required even when repeating the load application with stress relief (Fig. S4C).

Reproducing an interlocking pattern of pavement cells requires alternate positioning of differential stiffness along the periclinal walls

The simulations thus far indicate that locally increased stiffness of a periclinal wall segment at one side of a cell-cell border can displace the relative position of the anticlinal wall in the presence of turgor. To verify whether the observed deformation in the periclinal segments and displacement of the anticlinal wall can reproduce alternatingly positioned necks and lobes, finite element models of larger wall segments are developed to incorporate multiple, alternatingly placed regions of cell wall stiffening (Fig. 3G). To follow experimental observations on microtubule distribution, which presumably are translated to enhanced cellulose deposition, the stiffening regions on periclinal walls are extended in the depth of the anticlinal walls. The mesh of the finite element model is constructed with higher resolution near the cell borders for higher precision, and equal turgor pressures are

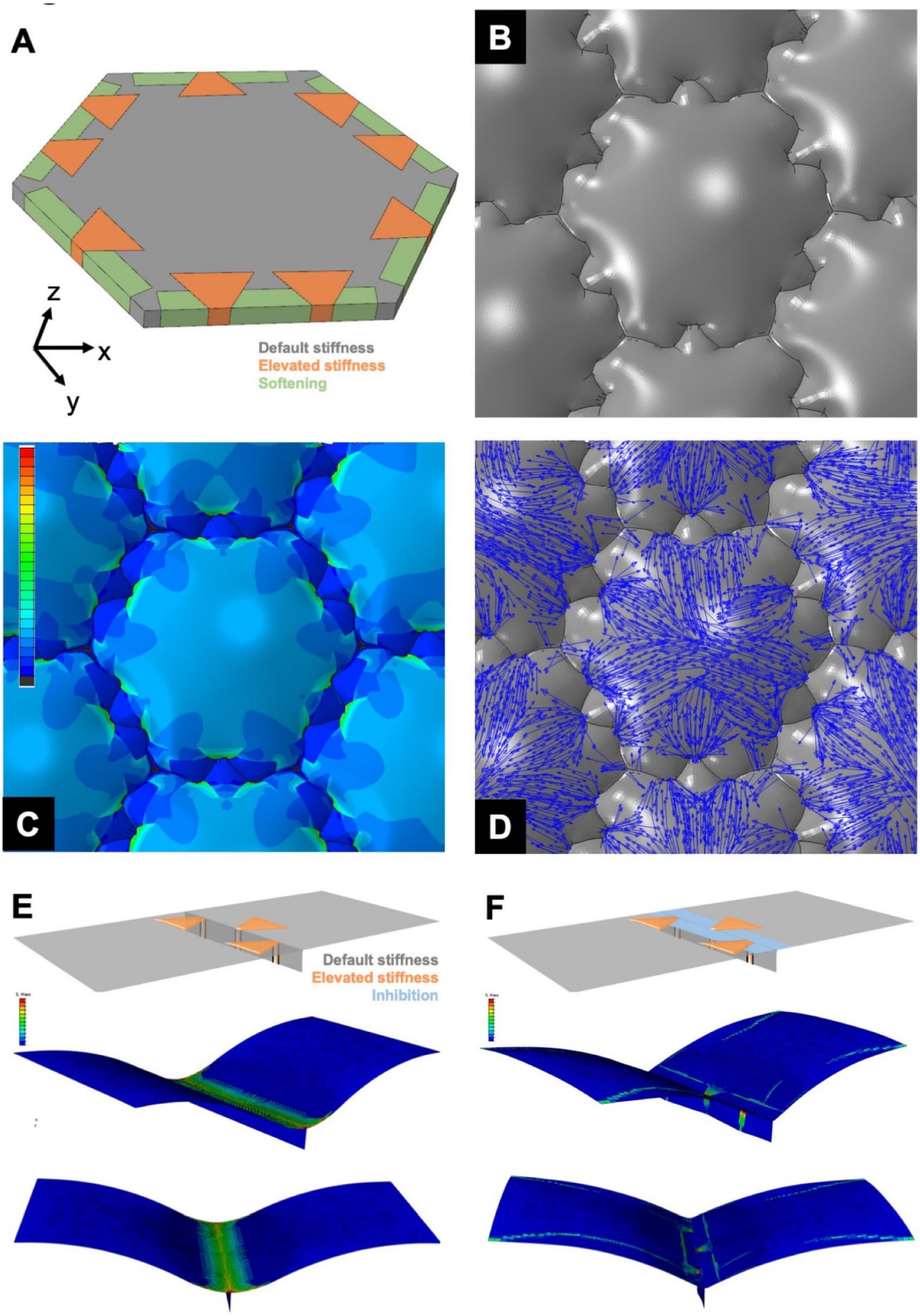

Fig. 4. Shape and stress development in pavement cells based on inhomogeneity in cell wall stiffness. **A)** Whole cell model considering local, alternating stiffening and softening of the inner and outer periclinal walls as well as extension of the stiffened regions in the anticlinal walls. **B-D)** Simulation of turgor induced deformation and stress in a model composed of multiple single-cell units as shown in **A**. The turgor pressure was set equal in all cells. **B)** Shaping of undulations. **C)** Stress pattern generated by turgor application in the periclinal walls and at periphery of tricellular junctions. Heatmap represents maximum principal stresses. **D)** Orientation of stress lines in periclinal walls. **E-F)** Incorporation of positive stress-stiffening feedback mechanism that amplifies stiffness based on local stress conditions starting from minute stiffness differential (ratio 1.01) in periclinal and anticlinal walls. Deformation and stress pattern after hundred iterations of load application. Heatmap represents von Mises stress. **E)** Without inhibition mechanism stiffness differentials even out. **F)** Inhibition of stiffening at alternating locations allows for stiffness differentials to amplify and undulations to form.

applied in both cells (Fig. 3H). To assess the magnitude of the shape forming effect, horizontal (in x direction) displacement of the mid-point of the anticlinal wall (A2) is recorded in each simulation (Fig. 3I). The results of the simulations show that one iteration of pressure application causes a displacement of the anticlinal wall that simulates the initiation of lobes and necks (Fig. 3J). The distribution of stresses reveals that regions of higher stress correspond to the regions with higher cell wall stiffness. To attain more pronounced lobes and necks, the process of turgor application is repeated. After each iteration, the deformed geometry (output) is used as initial geometry (input) for the next iteration, and wall stresses are readjusted to zero. The subsequent simulation is performed with all other parameters kept constant (Fig. S4D). This model shows how continuous deformation of the cell wall with localized alternatingly placed stiffness on two sides under turgor pressure can develop into lobes and necks.

Loosening of the cell wall promotes lobe outgrowth

It is thought that the delivery of new wall material and wall loosening enzymes on the lobe side of an undulation facilitates the expansion of lobe protrusions into the neighboring cells. The provision of this material is presumably mediated by arrays of actin microfilaments (Mathur and Hülskamp, 2002; Panteris and Galatis, 2005). To examine the effectiveness of wall loosening in generation of interdigitations, the finite element model is modified to allow for spatially confined softening of the cell wall. Similar to the stiffening, the softening is implemented either *ab initio* or *cum tempore*. The location of these softening regions is limited to the zones of the periclinal walls between the stiffened regions (Fig. 3K). As above, the triangular stiffened regions on periclinal walls are extended by narrow bands in the depth of the anticlinal wall. Simulations show that softening in the 'inter-neck' regions facilitates greater extension of the wall interdigitation in xy plane while the 'ballooning' of the periclinal walls in the Z direction is less pronounced compared to the simulations without the softening (Fig. 3L).

Extension of stiffening in the depth of the anticlinal walls enhances but cannot generate pavement cell lobes *de novo*

In the simulations above, the triangular stiffening regions in the inner and outer periclinal walls are connected by extensions of stiffened bands in the anticlinal walls. To investigate the influence of anticlinal wall stiffness extension, we modified this stiffening in the anticlinal wall to be only partially extended or absent and compared the displacement results with the full extension of the stiffened band (Fig. 3M). The simulations indicate that in the presence of periclinal wall stiffenings, undulations can be generated without stiffening in the anticlinal wall, but the magnitude of the undulations remain smaller compared to simulations with partially or fully extended stiffened bands in the anticlinal wall (Fig. 3I). Keeping all the other variables constant, the extension of stiffening into the anticlinal wall increases the magnitude of the formed lobe as measured by the relative displacement of point A2 (Fig. 3N).

The presence of anticlinal wall stiffening in the absence of local stiffening in the periclinal walls produces no deformation under application of turgor pressure. This is consistent with the simulations made using the isolated anticlinal wall model. This simulation, therefore, further emphasizes the dominant role of the periclinal wall in the formation of interdigitations.

Multi-cell simulation confirms that local stiffening and turgor-driven stretch of the cell wall can form interlocking pattern in the tissue context

To assess whether the concepts identified above hold for a multicellular context, a multicell finite element model is developed based on an arrangement of multiple, identical whole cell modules with hexagonal geometry and alternatingly located stiffness and softening zones on the periclinal walls (Fig. 4A-D). The periclinal stiffening regions in inner and outer walls are connected by stiffened bands extending in the depth of the anticlinal walls (Fig. 4A).

As in the previous sections, in this class of models a turgor pressure difference in adjacent cells is not necessary to generate the protrusions. The results indicate that highest stresses correspond to regions with a higher stiffness (neck) (Figs. 4B-D). Interestingly, the model predicts that stress lines extend between adjacent necks and cross each other in the center of the periclinal cell wall (Figs. 4D and S4E).

To investigate the effect of the geometry resulting from the local stiffening and softening of the periclinal walls on the stress pattern in the cell wall, we use the output geometry of the previous simulation as a new input model, but we implement isotropic and uniform material properties. The result of the subsequent load (turgor) application indicates that after the lobes and necks are formed, the geometry itself results in stress anisotropy with higher stresses in necks, even if their stiffness is the same as that of the lobe (Fig. S4F). This confirms the validity in 3D of predictions that had been made previously on a surface model focusing only on the periclinal walls (Sampathkumar et al., 2014).

A positive mechanical feedback loop based on stress-induced stiffening and lateral inhibition can shape pavement cells

Previously, we showed that if the stiffness ratio between the opposing necks and lobes is not sufficiently large, iterating the simulation with repeated load application cannot produce discernable displacements on cell borders if the stiffness ratio remains constant. However, a living cell is dynamic; it can increase cell wall stiffness by adding cellulose. The deposition of cellulose microfibrils is guided by microtubules, and microtubules orient along stress fields (Landrein and Hamant, 2013; Uyttewaal et al., 2012). In the previous section, we observed that, even if the cell material possesses a uniform stiffness value in all regions after the lobes and necks are initiated, the shape itself generates higher stresses at the convex sides of the undulations on the periclinal walls. We, therefore, investigated the effect of stress-driven microtubule bundling on the cell shaping process if a feedback mechanism is implemented in which the cell wall is gradually stiffened in regions with locally elevated stress. This is implemented over several iterations starting with an infinitesimally small initial stiffness difference in the periclinal wall segments (Figs. 4E and F). After each iteration, the model is set to update local stiffness values based on the presence of local stress (Fig. S6A). For this purpose, a Python

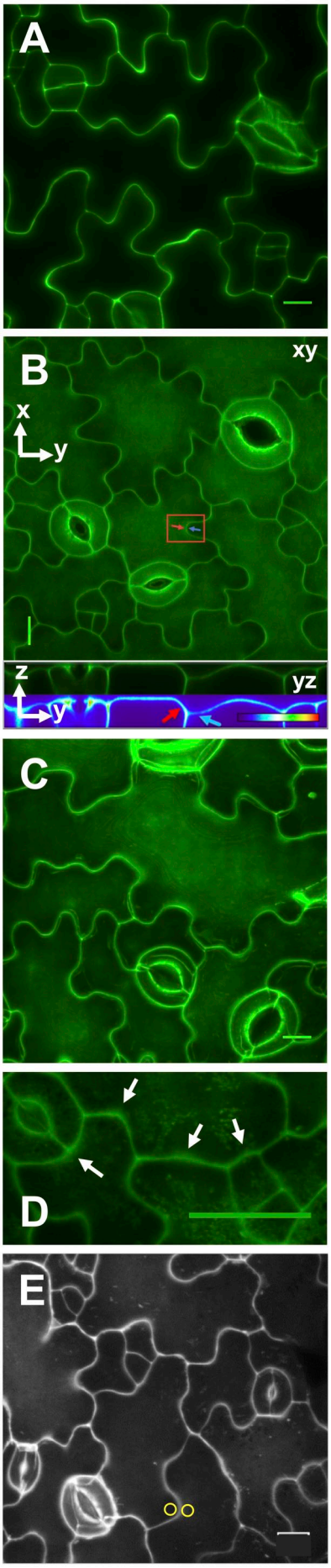

Fig. 5. Staining for de-esterified HG pectin in *Arabidopsis thaliana* cotyledons sampled 3 to 5 DAG. **A)** Single optical section through the center of the epidermal layer thickness stained with COS^{488} shows varying signal intensity along anticlinal walls and high signal intensity at tri-cellular cell junctions. **B)** Maximum projection of z-stack labeled with propidium iodide (top) and orthogonal single yz optical slice through same z-stack, crossing the center of the marked lobe and neck pair (bottom). **C)** COS^{488} show higher signal intensity at the neck side of the periclinal walls also visible in the yz orthogonal section taken at the location of the inset identified by the red rectangle in **B**, shown in monochrome and heatmap. **D)** Maximum projection of sample stained with COS^{488} shows that in smaller cells and along cell borders with barely developing bends, higher signal appears at the neck side of the periclinal wall. **E)** Maximum projection of z-stacks from COS^{488} stained sample. Circular regions of interests were placed on opposing sides of border waves to measure mean signal intensity for necks and lobes on the periclinal walls (see also Supplemental Information). Scale bars = 10 μm (**A, B and C, E**) and 20 μm (**D**).

code was developed to extract the stresses present at each element of the structure at the end of each iteration (output). Based on the local elemental stress, each element is assigned a new stiffness value calculated based on the previous stiffness value and the output stress resulting from the previous iteration.

The initial stiffness difference ratio implemented for this test is 1.01. The results indicate that the deformation upon the first iteration is relatively small and during subsequent iterations, the displacement of the lobe does not increase considerably but reaches a plateau with a negligible displacement (Fig. 4E). Stresses resulting from a single load application are not local enough to produce undulations through the feedback mechanism. Essentially, stresses are leveled out over the distances relevant here, and the feedback loop causes an increase in overall stiffness at the border of the two periclinal walls rather than sharpening the differences between neighboring lobe and neck regions.

We, therefore, tested whether adding an inhibitory mechanism could cause an augmentation in stiffness differential during feedback iterations. To implement this, feedback-driven stiffening is prevented in regions between the incipient necks, given as an input to the feedback model (Fig. 4F). Lobe formation is amplified by the feedback mechanism even when starting with very small stiffness differences between future necks and lobes (ratio 1.01, in other words, increase by 1%) (Figs. S6B and 4F). These results suggest that while a feedback loop starting from infinitesimally small stiffness differences does produce realistic results, it cannot be based on stress stiffening alone but needs to incorporate a mechanism that prevents stiffening at selected locations.

Experimental validation of *in silico* predictions

The models above predict that alternating changes in material properties of the cell wall at the site of undulations can produce an interlocking pattern in pavement cells. Changes in material properties suggest that variations in the biochemical composition of the cell wall are involved. To experimentally validate the predictions made by the simulations, we studied the spatial distribution of two major cell wall components known to modulate the mechanical properties of primary plant cell walls: cellulose microfibrils and homogalacturonan (HG) pectin. This was performed in the epidermis of *Arabidopsis* cotyledons.

Pectin is weakly esterified in neck regions

Our model predicts that the mechanical properties along the cell border vary in space, but it does not specify which biochemical component of the cell wall is responsible for this effect. Pectin de-esterification has been linked to changes in mechanical stiffness of the plant cell wall (Amsbury et al., 2016; Braybrook and Peaucelle, 2013; Carter et al., 2017; Chebli et al., 2012). We used COS^{488}, an oligosaccharide probe conjugated with Alexa Fluor 488 recently synthesized and reported to be highly specific for de-esterified HG pectin (Mravec et al., 2014). COS^{488} staining typically exhibits higher signals at tips of undulations at the anticlinal walls (Fig. 5A). Maximum intensity projections of z-stacks were used to capture all wall areas despite different z-positions in lobes and necks. The results indicate a pattern of de-

esterification in the periclinal walls with neck (indentation) side of a curvature exhibiting a higher signal (Figs. 5C, D and E). Interestingly, COS^{488} staining also showed bright spots at cell junctions (Fig. 5A). We hypothesize that de-esterification of pectin in the middle lamella might be employed at the junctions to strongly attach the neighboring cells to each other.

A recent study has shown that propidium iodide, a common chemical probe for cell wall staining, has a higher affinity for weakly esterified pectin compared to its highly esterified form (Rounds et al., 2011). We exploited this affinity of propidium iodide to investigate the variations in pectin chemistry in the walls of pavement cells. Living cotyledons of wild-type *Arabidopsis thaliana* taken from seedlings at 2-3, 4 and 5 days after germination (DAG) were stained using propidium iodide and observed under the confocal laser scanning microscope. At this developmental stage, pavement cells have already acquired wavy shapes but continue to grow (Zhang et al., 2011). In the anticlinal wall, the fluorescent signal intensity was typically higher at the tips of the undulations compared to the straight wall segments between two undulations (Fig. S5A). Maximum projections of z-stacks showed that in the periclinal walls, higher signal intensities were present on the neck sides of the undulations while at the lobe sides the signal was often dim (Fig. S5B). Quantitative comparison of the signal intensity difference between neck and lobe pairs ($n>100$) of different cells ($n=19$) of several cotyledons ($n=5$), showed a significant statistical difference ($p<0.00001$). The same result was obtained when analyzing orthogonal views (Fig. 5B). Based on the higher affinity of propidium iodide to de-esterified pectin, we hypothesized that pectin is weakly esterified at neck side of undulations.

Statistical analysis comparing the signal intensities between necks and lobes for both COS^{488}, a marker specific for weakly esterified pectin, and propidium iodide, showed higher signal at the neck side and the differences were significant ($p<0.0001$, Supplemental Information). While in this study we mainly focused on pavement cells between 2-5 DAG, this association was not limited to larger cells or already wavy wall segments. Indeed, we observed that walls with even a slight curvature in 2-5 DAG stage (Fig. 5D) or early stage pavement cells at 1 DAG (Fig. 5E, see also Supplemental Information) both exhibit a similar pattern on the neck side. However, due to challenges of working with early-stage cells such as staining the periclinal walls, we focused on day 2 after germination onwards. Even at this stage, cells are growing and new cells continue to appear as a result of cell division.

Cellulose microfibrils and microtubules form organized bundles at the neck sides

The pattern of stiffening in the periclinal and anticlinal walls of pavement cells can be mediated through coordinated positioning of cellulose microfibrils which in turn is thought to be controlled by microtubules. We, therefore, wanted to investigate the orientation of microtubules in pavement cells and used cotyledons of GFP lines MAP4 and TUB6 of seedlings between 3-5 DAG. Visualizing the microtubules beneath the outer periclinal wall down to half the thickness of the anticlinal wall showed strong bundling of microtubules in association with necks (Figs. 6A-C and S7D, S5C). While in lobes, microtubules could occasionally be observed, their occurrence in this location was scarce compared to necks. It seems that in central regions of cells, where bundles of microtubules arriving from multiple necks converge, the overall distribution of microtubules becomes random. A similar pattern was observed for stress lines in the multicell models as discussed earlier (Fig. 4D). We also used GFP-TUB6 line to confirm the observations (Fig. 6B, C and S7D). The results from GFP-TUB6 on microtubule distribution in the outer periclinal wall support the results for GFP-MAP4 pavement cells. The fan-shaped orientation of microtubules is more evident in GFP-TUB6 results compared to crowded GFP-MAP4. Interestingly, at some locations, microtubules appear to form bundles while the cell border appears to be only slightly bent. These sites were also associated with marked accumulations of microtubule label at the anticlinal walls (arrowheads marking the dotted microtubule on the red lines of cell borders in Fig. 6B). The inner periclinal walls showed a similar trend for the microtubules at locations of fully developed necks as well as for the relatively straight regions corresponding to arrowheads in Fig. 6B with a marked bundling of microtubules (Fig. 6C). We hypothesize that these regions may mark the locations for a strain/stress-driven positive feedback loop that result in fully-developed waves of lobes and necks. We hypothesize, as we will discuss later, that this focal polarization of microtubules is preceded by a mechanical symmetry breaking due to local cell wall buckling Further, away from the tip of the lobes, bundles of microtubules radiating from two adjacent necks form transverse bundles on the shank of the tube-like lobe (Figs. 6A). These arrays seem to connect regions of greatest stress which the FE model predicts will develop in the necks. If this results in increased cellulose deposition at these locations, this stiffening would restrict the widening of lobes and instead allows for their elongation. A finite element model shows that placement of stiffened necks produces stress fields that can eventually result in the orientation of microtubules that connect the opposing necks (Fig. 4D).

These conjectures on cell growth behavior based on the orientation of microtubules are based on the presumption that cellulose microfibrils are deposited at the same location and in the same orientation as cortical microtubules. In the majority of the earlier studies, microtubule orientation has therefore been used as a proxy for cellulose-mediated wall stiffening, although direct evidence was rarely provided. The reason for this is mostly technical since fluorescent labeling of cellulose in living cells covered by a cuticle remains a challenge. To study the distribution and organization of cellulose microfibrils in pavement cells, we used calcofluor white and Pontamine Fast Scarlet 4B (PFS) (Anderson et al., 2010) to stain the living cotyledons. PFS is reported to be highly specific for cellulose and has been used in high-resolution imaging of cellulose (Anderson et al., 2010; Liesche et al., 2013).

In confocal images of pavement cells stained with PFS or calcofluor white, a notable concentration of cellulose microfibrils was observed in the neck regions from where they form a divergent fan-shaped configuration in the outer periclinal walls (Figs. 6D, S5F, S5D and E, Movies S1 and S2). Statistical analysis revealed a significant difference in

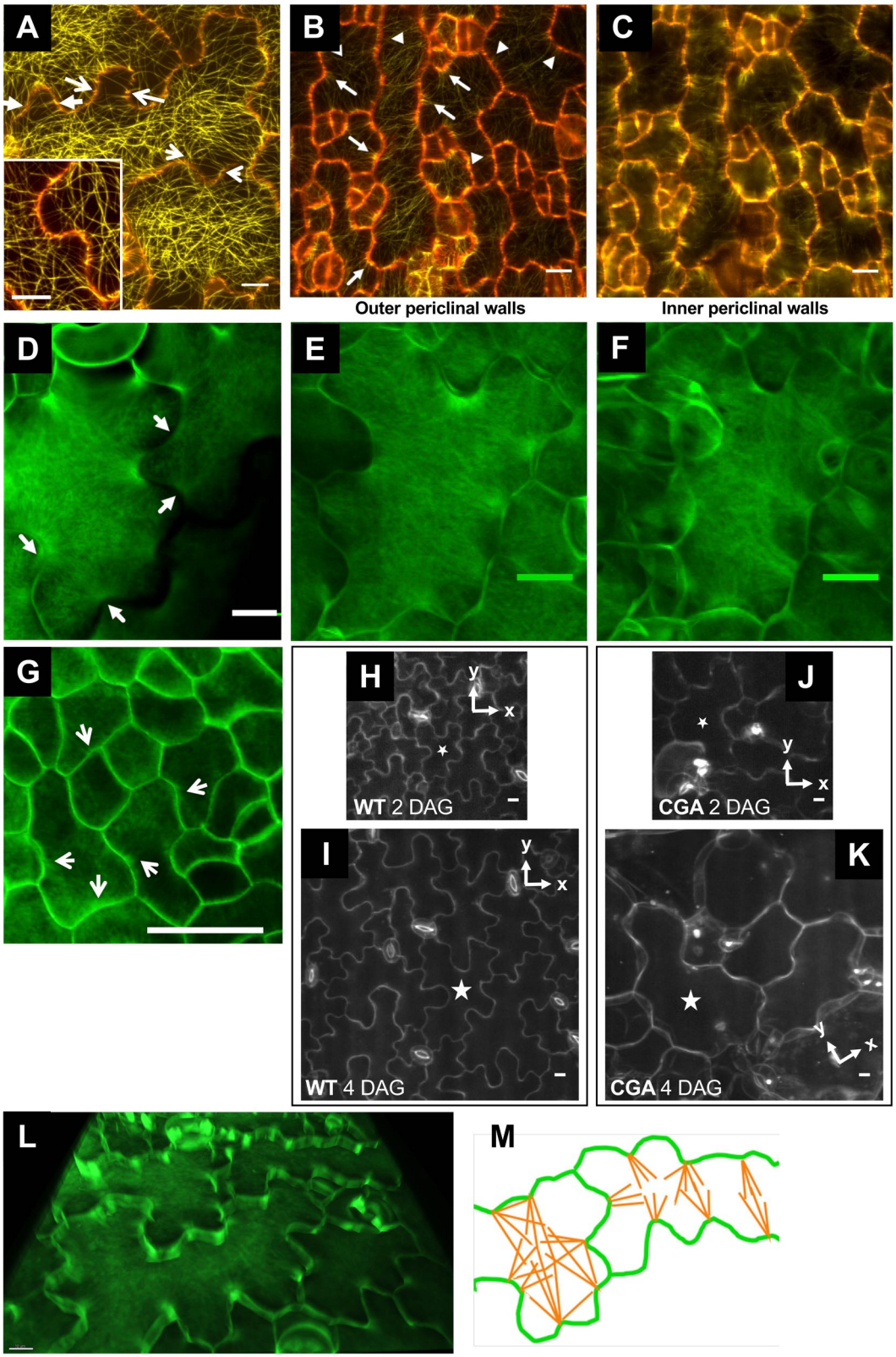

Fig. 6. Organization of microtubules (yellow pseudocolor) and cellulose microfibril (green pseudocolor). **A)** Microtubules labeled by GFP-MAP4 are abundant in association with the neck sides of undulations (maximum projection). Microtubules in the GFP-MAP4 line feature neck to neck connections forming circumferential hoops at the shank of lobes (pair of arrows, maximum projection). Inset shows higher magnification of a second sample. **B)** and **C)** Microtubules underlying the outer and inner periclinal walls, respectively, of the same pavement cells in the GFP-TUB6 line. Micrographs are maximum projections of the top **(B)** and bottom **(C)** halves of a z-stack. In **A-C** a single optical section from the center of the z-stack was pseudocolored in red to mark cell borders. **D-G)** Cellulose in pavement cells of *Arabidopsis thaliana* cotyledons at 3 to 5 DAG (**D,F**) and extracted from seed (**G**) stained with calcofluor white (for PFS label of cellulose see Supplemental Information). **D)** Cellulose microfibrils are concentrated at the necks from where they radiate into the periclinal wall (maximum projection, see also Figs. S5D-F and Movies S1 and S2). Cellulose microfibrils in outer (**E**) and inner (**F**) periclinal walls of the same cells. Micrographs show maximum projections of the top (**E**) and bottom (**F**) halves of a z-stack (see also S5H). **G)** Bundles of cellulose microfibrils in pavement cells of cotyledon extracted from the seed coat are associated with the necks of barely emerging curvatures. **H-K)** Time lapse of pavement cell morphogenesis of wild-type *Arabidopsis thaliana* cotyledons treated with DMSO (control) (**H,I**) and CGA (**J,K**) visualized at 2 and 4 DAG. Fluorescence is propidium iodide signal. While the DMSO-treated cells showed increase in surface area, perimeter and lobe number, the growing CGA-treated cells developed fewer lobes and necks (see Supplemental Information). The coordinate systems indicate the orientation of the mounted samples. **L)** Oblique view of a reconstructed z-stack of pavement cells showing that cellulose microfibrils extend into the depth of the anticlinal wall at neck-lobe pairs (see Movies S1 and S2). **M)** Schematic representation of typical cellulose orientation depending on the aspect ratio of cells: in elongated cell regions (right), the microfibrils form a pattern predominantly perpendicular to the long axis. In cell regions with an aspect ratio close to one (left), bundles of cellulose are more centrifugally oriented (see also Fig. 4D). Scale bars = 10 μm, 20 μm (G).

PFS signal between necks and lobes ($p<0.0001$, refer to Supplemental Information). Tips of lobes displayed considerably weaker signal and generally seemed devoid of organized microfibrils. However, similar to the organization of microtubules, microfibrils appear to connect neighboring necks (Fig. 6D, S5D-F). Similar to the organization of microtubules, in most pavement cells of seedlings between 2-5 DAG, the orientation of cellulose microfibrils in outer periclinal walls away from the undulations were mostly random in mid-regions exhibiting lower aspect ratios or dominantly transverse in narrow cell regions that were axially elongated (Figs. 6D, M and S5D and F). The association of cellulose bundles with neck (indentation) sides was not limited to pavement cells that display pronounced lobes. We

observed that even in pavement cells of cotyledons acquired prior to germination by removing the seed coat or just germinated, slight cell shape curvatures are already associated with radiating cellulose bundles (Fig. 6G).

To investigate the mechanical impact of the observed spatial distribution of cellulose microfibrils on wavy cell shape development, we experimentally reduced cellulose crystallinity and monitored the shape of the same cells in a time-lapse study. Reducing cellulose crystallinity is suggested to correlate with altered cell shapes and occurrence of a swollen phenotype (Aouar et al., 2010; Fujita et al., 2013). We grew Arabidopsis seedlings in presence of CGA 325'615 (CGA), shown to reduce cellulose crystallinity (Crowell et al., 2009; Peng et al., 2001), and monitored shape parameters over 4 DAG. At 2 DAG, cells in samples grown in media containing CGA (treated cell hereafter) and the control cells had the same perimeter and area (Supplemental Information). However, lobe formation in treated cells was significantly altered. Following the same cells over a period of 4 first days after germination showed that control cells had an average of 9.1 (± 0.7) lobes, whereas treated cells only developed 3.3 (±0.5) at 2 DAG. Over the two subsequent days (at 4 DAG), control cells formed 6-7 additional lobes, whereas CGA treated cells only added 1-2 lobes ($p<0.001$, see Supplemental Information for analysis and Fig. S8). These results indicate that interference with cellulose causes a significant reduction in lobe formation from early stages of epidermal cell development (Fig. 6 H-K). This further supports the significance of cellulose in development of wavy cell borders by restriction of expansion in the neck regions. Further, this emphasizes that the present model is not limited to cells that are already highly wavy and that this mechanism is essential also lobe formation at earlier stages of development.

Acquiring images of the cellulose orientation in the inner periclinal walls proved challenging due to the thickness of the samples and the fact that the signal from the inner periclinal walls was challenging to distinguish from the signal deriving from the directly adjacent mesophyll cell walls. However, in some cases, we succeeded and observed that the cellulose enrichment and orientation on the inner periclinal wall seems to mirror the outer periclinal wall (Figs. 6E, F and S5H). This motivated us to analyze the cellulose status of the anticlinal walls since they might serve as mechanical links between the inner and outer faces of pavement cells.

Cellulose microfibrils and microtubules form bundles at the undulations that extend in depth of the anticlinal walls coupling the inner and outer walls

3D reconstruction of confocal images of cotyledons stained with calcofluor white revealed that in neck regions cellulose extends down the anticlinal walls (Fig. 6L, Movie S2). This can also be observed by orthogonally slicing the z-stack and acquiring maximum X or Y projections for narrow segments (Figs. S5F1 and F2). These observations provide support for the predictions made by the finite element model incorporating alternate placement of stiffness on periclinal walls. As the finite element simulations show, the anticlinal extension of cellulose microfibrils at the undulation can act as a lever, increasing the magnitude of undulations.

Regardless of the mechanical contribution of the anticlinal reinforced bands in the development of undulations, they might transmit the mechanical signal from the inner periclinal wall up to the outer periclinal wall. To visualize this, we used the finite element model with the extension of stiffening in the depth of the anticlinal wall but without stiffened regions on the periclinal wall (Fig. 7A). Although this configuration does not generate any undulation in the anticlinal wall, the stress can be partly transmitted to the periclinal wall at its junction with the anticlinal bands. This can mark the position, attract further bundling of cortical microtubules in a positive feedback loop, and lead to deposition of cellulose under the outer periclinal wall. Since the stress due to local stiffening of the inner periclinal wall can be transmitted to the anticlinal walls (Fig. 7B), these bands of anticlinal stiffening can originate from the stress generated from the inner periclinal wall. This may explain why, if one of the periclinal walls develops a particular pattern of anisotropy, the other wall is triggered to mirror this through the microtubule-mediated addition of cellulose microfibrils. The stress pattern would be propagated from one periclinal wall to the other by way of the anticlinal walls.

Interestingly, after removal of the optical slices pertaining to periclinal walls to reveal the anticlinal wall, 3D reconstruction of the confocal stack shows that cortical microtubules assume a preferentially vertical (Z direction) orientation on the anticlinal walls (Figs. 7C and D, Movie S3). Since microtubules are thought to orient predominantly in direction of maximal stress, the vertical orientation corroborates the presence of a stress pattern oriented predominantly perpendicular to the plane of the leaf, as predicted by our finite element model (Figs. 3A-C). This suggests that putative stresses due to "tissue-level" forces that would be inherently parallel to the leaf surface in the anticlinal walls, even if present in leaf epidermal cells, are overridden by substantial cell-level turgor-generated stresses. Importantly, we observed that distribution of microtubules on the anticlinal walls are non-uniform and the microtubules are enriched near the locations of necks. Projecting the anticlinal microtubule signal from a 3D z-stack onto a 2D plane can render the precise localization of microtubules challenging. This is because microtubule-enriched regions placed alternatingly on two sides of the thin anticlinal wall can become impossible to associate with one side or the other. 3D visualization of microtubules (Movies S3 and S4) and specifically using dual channel 3D reconstructions (with propidium iodide marking the cell wall, Movie S4) was particularly helpful to determine microtubule localization relative to the adjacent anticlinal wall, particularly so in case of early stage bends (shallow bends marked in Movie S5). Our analysis of microtubule density between lobes and necks demonstrated that in the majority of cases, microtubules are enriched on the neck sides of the anticlinal walls, coinciding with microtubule bundling under periclinal wall necks ($p<0.0001$) Thus, microtubule association with necks is not limited to periclinal walls. It is important to note that, to observe the nuances of microtubule density variation on anticlinal walls, proper exposure and image processing is crucial.

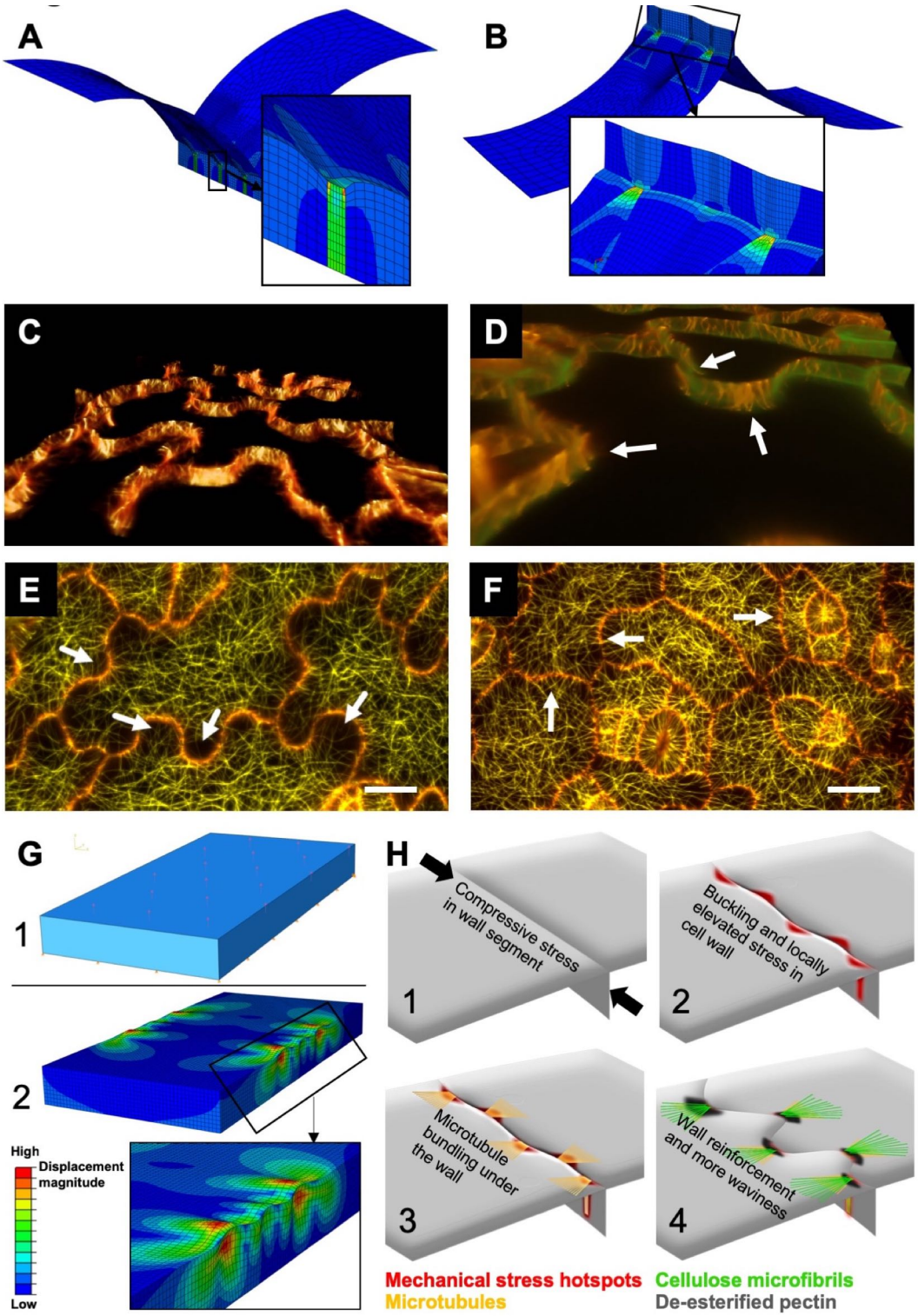

Fig. 7. Patterns of mechanical stress and microtubule orientation. FE models containing a segment of anticlinal and periclinal walls under turgor pressure show that **A)** anticlinal bands of stiffened cell wall material and homogeneous isotropic periclinal wall or **B)** material inhomogeneity in the periclinal wall can cause locally elevated stress in the connected wall transmitting stress between the inner and outer cell walls. **C)** Oblique view of a z-stack 3D reconstruction of pavement cells from *Arabidopsis thaliana* GFP-MAP4 line excluding periclinal walls demonstrating cortical anticlinal microtubules. **D)** Dual channel image of propidium iodide (green) and GFP-MAP4 (orange) showing that cortical anticlinal microtubules appear more abundantly at the neck side of the undulations. **E** and **F)** Cortical periclinal microtubules visualized in cotyledons of the *Arabidopsis thaliana* GFP-MAP4 line at 4 (**E**) and 1 DAG (**F**). At both stages, microtubule density at opposite sides of corresponding lobe-neck pairs is different with higher density at the neck side. However, this difference is less pronounced at earlier developmental stages (white arrows in **F**). At 4 DAG microtubules appear to be bundled in necks while they are scarce in lobes. Occasionally microtubule bundles reach the tips of a lobe. The images do not correspond to the same cotyledon. Maximum projections of z-stacks. Scale bars = 10 µm. **G) G-1)** Closed-box model of a brick shaped cell with turgor pressure applied to inner face of the outer periclinal wall. Turgor pressure was not applied to lateral walls as equal pressures were shown in previous models to cancel each other out in a multicell context and only result in compression of the wall thickness. Inner periclinal wall was prevented from out or inward displacement to simulate attachment to mesophyll layer. **G-2)** Buckling mode from the linear buckling analysis demonstrating folding of the cell border in both periclinal and anticlinal walls. Interestingly, the model suggests the location of indentation on periclinal walls to bulge out of plane which is consistent with microscopic observations of pavement cells. **H)** Schematic of the proposed multi-step process initiating pavement cell morphogenesis. **H-1)**. Compressive stress in anticlinal walls arises due to internal pressure bulging out periclinal walls. **H-2)** Stress inhomogeneities arisen due to buckling create stress hotspots that trigger local bundling of microtubules (**H-3**), alterations in pectin esterification and reinforcement of the cell wall by cellulose deposition. Feedback mediated cellulose deposition leads to further expansion of lobes (**H-4**).

Mechanical buckling may precede polarization and symmetry breaking

We observed that microtubules appear to be bundled in necks in regions with an already established curvature, while they are scarce in lobes and only occasionally do cortical microtubule arrays seem to stretch into the tip of lobes (Fig. 7E). This confirms microtubule behavior in pavement cells observed by Armour et al. (2015). In smaller, less developed cells or regions of developed cells with walls with smaller bends, however, the difference in microtubule density on two sides of the wall between lobes and necks appears to be significantly less pronounced compared to later stages (Fig. 7F). Our analysis plotting the difference in microtubule

numbers across the wall versus the degree of wall curvature (as a measure of lobe progression) revealed a moderate correlation (r=0.5, see Supplemental Information). This is consistent with the notion proposed here, that microtubule bundling and consequent wall reinforcement can amplify the amplitude of undulations in a positive feedback loop. However, it may also imply that lobe initiation can precede the focal bundling of microtubules and cell content polarization. In such a scenario, the initial bundling of microtubules at necks, which we demonstrated to experience higher stresses, would initially imply a correlation rather than a causality in lobe formation.

Our simulations suggested that while the anticlinal walls experience large positive (tensile) stresses in z-direction due to the shape and dimensions of the inflated cells, the stress along the length of the anticlinal wall can become locally zero or negative (compressive). This is interesting as the plant cell wall in turgid cells is commonly presumed to be ubiquitously under tension. Based on our observations, we hypothesize that in the anticlinal walls and consequently in the connected periclinal walls, local compression and buckling may occur. For proof of concept, we developed an FE model of a closed-box rectangular cell geometry subject to internal pressure (Fig. 7G-1) (see Supplemental Information). Positive eigenvalues were found from the linear buckling analysis suggesting that compressive stress and buckling can arise due to cell geometry and internal pressure. A buckling mode for this model is depicted in Fig. 7G-2. Interestingly, the model also suggests the periclinal wall at site of indentations to locally bulge out (magnified view 7G-2). This is consistent with the microscopic observations showing the cell wall on neck side of undulations bulging out of plane (Fig. 1A and orthogonal view in Fig. 5B). These results indicate that the cell walls have the potential to buckle due to cell geometry and internal pressure.

Discussion

Unlike animal cells, in plant cells actin-myosin based actuators are not directly involved in generating the forces required to move or alter cell shape. In this study, we show that complex cell shaping in plants is correlated with sophisticated mechanical modification of the cell wall. Interlocking protrusions in leaf epidermal cells are common traits in many plants and have attracted considerable attention since neither the events underlying the genesis of these shapes nor their purpose is understood (Jacques et al., 2014; Vofely et al., 2018). The analysis of the underlying molecular pathways and the characterization of the roles of cytoskeletal activities and cell wall biosynthesis have presented a formidable challenge to biologists and modelers (Armour et al., 2015; Belteton et al., 2017; Fu et al., 2005; Majda et al., 2017; Panteris and Galatis, 2005; Sampathkumar et al., 2014; Sapala et al., 2018; Sotiriou et al., 2018; Xu et al., 2010; Zhang et al., 2011). Until now, the focus of research has predominantly been on the localization of the cytoskeletal components and evaluating their contribution to cellular "lobiness" (Armour et al., 2015; Belteton et al., 2017; Fu et al., 2005), whereas experimental evidence for events pertaining to the cell wall and a mechanical explanation for the genesis and development of the interlocking cellular protrusions have remained largely elusive. A study by Sampathkumar et al. (2014) analyzed the correlation between cell wall stress and microtubule organization in pavement cells, albeit *post facto*, i.e. in cells that were already wavy. While this study crucially augments our existing knowledge on a link between microtubule organization, cell shape and mechanical stress, it does not inform us on the shaping of these cells. Here, we focused on upstream events to answer how cell shapes are formed *de novo* and how these shapes develop. Based on our experimental data and mechanical modeling we propose a new paradigm in which the development of cell shape is a product of initially minute material inhomogeneity and stress that are subsequently amplified through a feedback mechanism. Our simulations and microscopic observations of microtubule arrangement suggest that stress anisotropy can initiate the complex shaping process and act as a cell-scale morphogen.

Our initial simulations based on isolated anticlinal walls indicate that the mechanics of epidermal cells and specifically the stress state in the cell wall cannot be adequately addressed without taking the periclinal walls into account. We showed that a stretch-based model of an isolated anticlinal wall as proposed by Majda et al. (2017) is not realistic and can only produce near imperceptible bends, and that periclinal walls virtually eliminate these (Bidhendi and Geitmann, 2019).

Simulations including the periclinal walls on the other hand generate crucial and non-intuitive information. When turgor pressure is applied to all walls in a complete 3D model, with the cell dimensions typical for epidermal cells of *Arabidopsis,* the periclinal walls bulge out and the anticlinal walls are pulled inward reducing the in-plane projected cell surface. This can occur despite the exertion of the same pressure on the anticlinal walls. The reason for this is that due to difference in surface areas, the combined forces resulting from the turgor pressure on the periclinal walls are higher than those acting on the anticlinal wall surface. These simulations also imply that for a cell to grow in-plane, selective and isotropic softening of the anticlinal walls is not sufficient and changes in mechanical properties of periclinal walls are required. As the degrees of bulging and contraction depend on the relative surface areas of the periclinal and anticlinal walls of a given cell, this result implies that formation of a protrusion into a neighboring cell cannot be used directly as evidence for a turgor differential the cells. It could simply be generated by different cell geometries.

Another important conclusion obtained from 3D cell models is the finding that anticlinal walls experience high stresses vertically (in the Z direction) compared to the in-plane directions (Figs. 3B and C). This stress pattern matches the net orientation of cortical microtubules underlying the anticlinal walls. This suggests that anticlinal walls become reinforced anisotropically by cellulose microfibrils starting at the very early stages, upon formation and fusion of the cell plate. This anisotropic reinforcement enables the anticlinal walls to grow in their longitudinal direction, perpendicular to the net orientation of microfibrils, allowing growth of pavement cells in-plane while preventing their out-of-plane expansion (Figs. S7A-C, Movies S3 and S4).

Our simulations suggest that the formation of alternately located, non-yielding (stiff) regions on periclinal walls in a growing cell suffices to develop necks and lobes. We show

that this alternating pattern of stiffness distribution is consistent with cellulose deposition, associated with de-esterification of pectin. The stiff regions form into indentation or necks. Our simulations show that once lobes and necks are initiated, the geometry itself will cause the appearance of elevated stress at the neck side (Fig. 4D) even if isotropic material properties are used. The locations of elevated stress and the anisotropic stress pattern obtained through static simulation closely match the experimental observations of cortical microtubule bundling in necks and their orientation (Figs. 4D, 6A, 7E and D). This model can mechanically explain why pharmacological interference with cortical microtubule bundling has the potential to produce pavement cell phenotypes with reduced waviness (Armour et al., 2015; Fu et al., 2005; Mathur, 2004).

In the positive mechanical feedback loop between local wall stress and stiffness, we demonstrate that developing lobes and necks can initiate from infinitesimally small stiffness differentials if a stress-stiffening mechanism with lateral inhibition is incorporated. The existence of such a lateral inhibition mechanism seems to find an immediate biological equivalent in the proposed antagonism and competition between microtubule and actin regulation pathways (Chen et al., 2015; Fu et al., 2005; Fu et al., 2002; Xu et al., 2010). Since microtubules are associated with guided deposition of cellulose and actin filaments are thought to deliver new, and presumably softer, wall material, such a scenario would cause lateral inhibition of stiffening predicted by our model. The antagonistic pathways and, specifically, the exclusivity of actin to lobes are not uncontested, however (Armour et al., 2015; Belteton et al., 2017). For instance, Armour et al. (2015) did not observe any obvious association between lobes and actin microfilaments at least in early stages of pavement cell shape development. Therefore, the roles and the competition between the cytoskeletal elements in driving the progression of cellular protrusions warrants further investigation.

Further in the shank of lobes, bundles of microtubules radiating from two neighboring necks form transverse connections crossing the shank of the sinus-shaped lobe (Figs. 6A-C, and S7D). This structural pattern matches the stress pattern predicted by our finite element model (Fig. 4D and S4E). This cortical microtubule array is clearly translated into wall structural features as cellulose is enriched at these locations (Figs. 6D, S5D-F) presumably restricting further widening of lobes while promoting elongation thus generating an anisotropic growth pattern. These results are consistent with anisotropic strain patterns reported by Elsner et al. (2018).

Staining the cotyledons with propidium iodide and COS^{488} shows pectin in pavement cells to be weakly esterified at the neck sides of undulations. De-esterified pectin can enhance the mechanical stiffness of the pectic network when cross-linked by calcium. Therefore, changes to the pectin status in the neck region could have a direct consequence for local cell wall stiffness in periclinal walls. Variations in the esterification status of pectin have been implied in other plant tissues related to the polar growth of cells and organogenesis (Bidhendi and Geitmann, 2016; Palin and Geitmann, 2012; Peaucelle et al., 2015; Wolf et al., 2009). Moreover, it is possible that de-esterification of pectin in necks locally decreases cell wall deformability by preventing slippage and separation in the xyloglucan-cellulose network thus locally impeding cell wall growth (Abasolo et al., 2009).

Staining cotyledons with calcofluor white and PFS revealed bundles of cellulose microfibrils radiating from the neck side of the undulations. Accumulation and bundling of cellulose microfibrils in these regions can be interpreted as locally elevated stiffness of the cell wall. This is due to a considerable tensile stiffness of cellulose bundles compared to other cell wall polysaccharides. The tips of lobes on the periclinal walls showed considerably less fluorescent signal and generally seemed devoid of organized cellulose microfibrils. Similar to the organization of microtubules, microfibrils seemed to connect neighboring or opposite necks (Fig. 6D). In some observations, the neck-neck connections in the inner periclinal walls appeared to be more pronounced, and bundles of cellulose seemed packed tighter compared to their corresponding outer periclinal wall (Figs. 6E and F and S5H). Therefore, the inner periclinal wall may be more determinant in dictating the augmentation of undulations while the outer periclinal wall may loosely mimic the cellulose pattern of the inner wall. Such harmonization is possible by stress and strain coupling through the formation of anticlinal strips of cellulose reinforcement. Alternatively, the observed stronger neck to neck associations and tighter bundling in the inner periclinal walls may reflect a temporal order of events with the development of anisotropic reinforcement in the inner wall of a cell preceding that in the outer periclinal wall.

Armour et al. (2015) report that the regions of the anticlinal wall where microtubules form the cortical anticlinal bundles mark the position of incipient necks. However, our observations and a closer analysis of images provided by Armour et al. (2015) suggest that even the earliest evidence of microtubules focally marking a region of the anticlinal wall is associated with an already existing local change of curvature, even if not very prominent. Therefore, the available studies cannot indicate whether there was a change in the cell wall composition/stress that caused bundling of the microtubules in those regions or whether it was the microtubule accumulation that predicted the site of future lobes. Importantly, however, we observed that the change in microtubule density on the two sides of an undulation is a gradual process and the difference is imperceptible for slight wall curvatures (Fig. 7E and F). We suggest that the initial difference in microtubule density is a response to a difference in mechanical stress on two sides of an undulation. Our new hypothesis considers this stress difference to result from an event that has already formed the slight wave in the wall without a need for microtubule or consequently cell wall anisotropy, buckling. Buckling is a mechanical instability that occurs when structures lose their axial load-bearing capacity under compressive stress states resulting in formation of bends. Here we suggest this mechanical phenomenon to act at subcellular level as a morphogenetic step and a polarizer preceding the emergence of cell wall stiffness heterogeneity that would result in spontaneous and stochastic formation of local stress hotspots (Figs. 7G and H) and eventually leads to the formation of complex cell shapes. We provide a proof of concept for the notion that buckling in the walls can simply result from compressive stresses arising from cell geometry

and turgor (Fig. 3C). Localized stress can then trigger microtubule bundling and, as explained earlier, acting in a positive feedback loop, can result in cell wall reinforcement through local cellulose reinforcement. A schematic of the proposed morphogenetic steps summarizes the events in Fig 7H. This concept does not exclude that independently, and compounding this effect, external compressive stresses may arise due to conditions such as variations in growth rates between neighboring cells. Indeed Armour et al. (2015) and Elsner et al. (2012) demonstrated that cell wall growth rates can vary considerably between neighboring pavement cells as well as in different regions of an individual cell.

Our proposed model based on buckling as a separate mechanical event preceding cytoskeletal and cell wall biochemical polarization also provides a crucial explanation for phenotypes observed in pavement cells subjected to microtubule-related treatments or mutations. Interference with the regulators of microtubule functioning such as brassinosteroids, regulators of ROPs such as RhoGDIs, mutations in microtubule-associated or microtubule-severing proteins such as IQD, CLASP or KATANIN all considerably decrease but in no case do they completely eliminate cellular protrusions (Akita et al., 2015; Ambrose et al., 2011; Fu et al., 2005; Han et al., 2015; Kirik et al., 2007; Kotzer and Wasteneys, 2006; Liang et al., 2018; Lin et al., 2013; Liu et al., 2018; Mitra et al., 2018; Möller et al., 2017; Wu et al., 2013). The same applies to mutations affecting the actin cytoskeleton (Le et al., 2006; Rosero et al., 2016) or cellulose synthesis or crystallinity such as any1 or our CGA treatments (Fujita et al., 2013; Ivakov and Persson, 2013). In other words, neither interference with cytoskeletal elements nor alteration of the wall composition result in completely straight borders. This further corroborates the notion that microtubules and subsequent cellulose reinforcement of necks, while crucial in pavement cell development, do not initiate cell border waviness, further supporting our proposed model for morphogenesis of pavement cells.

Experimental Procedures

Plant growth conditions

Arabidopsis thaliana ecotype Col-0 seeds were germinated in sterile Petri plates containing 1X MS (Murashige and Skoog, 1962) media with 1% sucrose and 0.8% plant agar under long-day lighting condition. The seeds for GFP-expressing line GFP-TUB6 (Nakamura et al., 2004) was obtained from Arabidopsis Biological Resource Center, under stock number CS6550. The GFP-MAP4 line (Marc et al., 1998) was also used to verify the observations with GFP-TUB6.

Staining

Staining procedures were carried out mostly in dark condition. For pectin, seedlings were stained with either propidium iodide or COS^{488}. COS^{488} was generously provided by Dr. William George Tycho Willats (University of Copenhagen). For visualizing cellulose, calcofluor white and PFS, a dye with a high affinity to cellulose, were used. Calcofluor was used at a concentration of 2 mg/mL in ddH_2O. PFS staining was carried out with a 14 mg/mL solution of PFS in PBS buffer (Na_2HPO_4 3.2 mM, KH_2PO_4 0.5 mM, NaCl 135 mM, KCl 1.3 mM, pH 7.3).

CGA treatment and time-lapse study of pavement cell growth

Cotyledon samples from *Arabidopsis* were treated with the herbicide CGA (CGA 325'615) at 0.9 nM prepared from a 10 µM stock solution dissolved in DMSO. CGA is suggested to inhibit the synthesis of and reduce the cell wall content of crystalline cellulose (Peng et al., 2001).The same concentration of DMSO (v/v) was used for the control experiment. The solutions were added to the ½ x MS (Murashige and Skoog, 1962) growth media. The samples were labeled with propidium iodide (0.01 mg/ml) for 20 min, followed by three washes with distilled water before observation. Propidium iodide labeling was applied at each time point prior to observation. Samples were mounted between slide and coverslip at each image acquisition. After each image acquisition, samples were placed immediately back to the in vitro growth chamber. At each time point, the same cells were located and traced. The adaxial side of the wild-type *Arabidopsis* was chosen for the study. For statistical analysis, for each time-point, 50-70 cells were studied from 10-12 seedlings.

Fluorescence microscopy

Fluorescence microscopy was carried out on a Zeiss LSM 510 META confocal laser scanning microscope using a Plan Apochromat 63x oil immersion objective with numerical aperture of 1.40. For propidium iodide and PFS, excitation wavelength of 532 nm and bandpass emission filter of 550-615 nm was used. For COS^{488}, 489 nm laser with bandpass filter of 550-615 nm was used. For calcofluor white, excitation wavelength of 405 nm in META mode and bandpass filter of 420-480 nm was used. For GFP lines, either excitation wavelength of 489 nm with emission bandpass of 500-525 nm, or in META mode, the argon laser of 488 nm with bandpass filter of 505-550 nm were used. For time-lapse imaging of CGA-treated and control samples, LSM 5 LIVE was used with 532 nm laser with an emission filter 590-625 nm.

Image analysis and 3D reconstruction software

Analysis of fluorescence intensity was performed on maximum projections of z-stacks using ImageJ (Schneider et al., 2012). 3D reconstruction of confocal z-stacks was carried out using either Amira 5.6.0 (FEI, Visualization Science Group) or Bitplane Imaris 7.5.2 (Bitplane A.G.). Supplemental Movies were created using the volumetric rendering function of Imaris software on z-stacks acquired from the confocal microscope. For measurements and statistical analysis pertaining to cell wall components or microtubules refer to the Supplemental Information.

Modeling

Finite element simulations

Abaqus 6.14-2 finite element package was used for the creation of the geometries, meshing and post-processing. Abaqus/Standard solver was used for quasi-static finite element simulations (see Supplemental Information on modeling procedures and Abaqus, 2014 user manual for more details).

Feedback loop

To implement a feedback loop, a Python script was developed to read and write in the finite element model. After each iteration, the code extracts the deformed geometry from the Abaqus database and reads the stresses for each element. If a specific element has a stress higher than a threshold and does not belong to a list of stiffening-inhibition zone, the new value of stiffness for that element is updated in a stress-stiffening paradigm (see Supplemental Information on modeling procedures).

Author contributions

A.J.B. and A.G. designed the study, A.J.B. performed the modeling and the experiments. B.A provided the CGA treatment results. A.J.B., F.P.G, and A.G. analyzed the data, A.J.B. and A.G. wrote the manuscript.

Acknowledgments

This project was supported by a Discovery grant from the Natural Sciences and Engineering Research Council of Canada (NSERC) and by the Canada Research Chair Program. We would like to thank Dr. William George Tycho Willats and Dr. Jozef Mravec from the University of Copenhagen for kindly providing us with COS488 for pectin staining. We thank those colleagues who have provided constructive comments on previous versions of this manuscript as these helped us to improve this work.

References

Abaqus, V. (2014). 6.14 Documentation. Dassault Systemes Simulia Corporation.

Abasolo, W., Eder, M., Yamauchi, K., Obel, N., Reinecke, A., Neumetzler, L., Dunlop, J.W., Mouille, G., Pauly, M., and Höfte, H. (2009). Pectin may hinder the unfolding of xyloglucan chains during cell deformation: implications of the mechanical performance of *Arabidopsis* hypocotyls with pectin alterations. Molecular Plant *2*, 990-999.

Akita, K., Higaki, T., Kutsuna, N., and Hasezawa, S. (2015). Quantitative analysis of microtubule orientation in interdigitated leaf pavement cells. Plant Signaling & Behavior *10*, e1024396.

Ambrose, C., Allard, J.F., Cytrynbaum, E.N., and Wasteneys, G.O. (2011). A CLASP-modulated cell edge barrier mechanism drives cell-wide cortical microtubule organization in *Arabidopsis*. Nature Communications *2*, 430.

Amsbury, S., Hunt, L., Elhaddad, N., Baillie, A., Lundgren, M., Verhertbruggen, Y., Scheller, H.V., Knox, J.P., Fleming, A.J., and Gray, J.E. (2016). Stomatal function requires pectin de-methyl-esterification of the guard cell wall. Current Biology *26*, 2899-2906.

Anderson, C.T., Carroll, A., Akhmetova, L., and Somerville, C. (2010). Real-time imaging of cellulose reorientation during cell wall expansion in *Arabidopsis* roots. Plant Physiology *152*, 787-796.

Aouar, L., Chebli, Y., and Geitmann, A. (2010). Morphogenesis of complex plant cell shapes: the mechanical role of crystalline cellulose in growing pollen tubes. Sexual Plant Reproduction *23*, 15-27.

Armour, W.J., Barton, D.A., Law, A.M., and Overall, R.L. (2015). Differential growth in periclinal and anticlinal walls during lobe formation in *Arabidopsis* cotyledon pavement cells. The Plant Cell *27*, 2484-2500.

Baskin, T.I. (2005). Anisotropic expansion of the plant cell wall. Annual Review of Cell and Developmental Biology *21*, 203-222.

Baskin, T.I., Beemster, G.T., Judy-March, J.E., and Marga, F. (2004). Disorganization of cortical microtubules stimulates tangential expansion and reduces the uniformity of cellulose microfibril alignment among cells in the root of *Arabidopsis*. Plant Physiology *135*, 2279-2290.

Baskin, T.I., Wilson, J.E., Cork, A., and Williamson, R.E. (1994). Morphology and microtubule organization in *Arabidopsis* roots exposed to oryzalin or taxol. Plant and Cell Physiology *35*, 935-942.

Belteton, S., Sawchuk, M.G., Donohoe, B.S., Scarpella, E., and Szymanski, D.B. (2017). Reassessing the roles of PIN proteins and anticlinal microtubules during pavement cell morphogenesis. Plant physiology, pp. 01554.02017.

Bidhendi, A.J., and Geitmann, A. (2016). Relating the mechanics of the primary plant cell wall to morphogenesis. Journal of Experimental Botany *67*, 449-461.

Bidhendi, A.J., and Geitmann, A. (2018). Finite element modeling of shape changes in plant cells. Plant Physiology *176*, 41-56.

Bidhendi, A.J., and Geitmann, A. (2019). 3D geometry matters–mechanical modeling of cellular morphogenesis. Developmental Cell, Accepted for publication.

Braybrook, S.A., and Peaucelle, A. (2013). Mechano-chemical aspects of organ formation in *Arabidopsis thaliana*: the relationship between auxin and pectin. PLoS One *8*, e57813.

Burgert, I., and Fratzl, P. (2009). Plants control the properties and actuation of their organs through the orientation of cellulose fibrils in their cell walls. Integrative and Comparative Biology *49*, 69-79.

Carter, R., Woolfenden, H., Baillie, A., Amsbury, S., Carroll, S., Healicon, E., Sovatzoglou, S., Braybrook, S., Gray, J.E., and Hobbs, J. (2017). Stomatal opening involves polar, not radial, stiffening of guard cells. Current Biology *27*, 2974-2983. e2972.

Chebli, Y., Kaneda, M., Zerzour, R., and Geitmann, A. (2012). The cell wall of the *Arabidopsis* pollen tube—spatial distribution, recycling, and network formation of polysaccharides. Plant Physiology *160*, 1940-1955.

Chen, J., Wang, F., Zheng, S., Xu, T., and Yang, Z. (2015). Pavement cells: a model system for non-transcriptional auxin signalling and crosstalks. Journal of Experimental Botany *66*, 4957-4970.

Cosgrove, D.J. (2005). Growth of the plant cell wall. Nature Reviews: Molecular Cell Biology *6*, 850-861.

Cosgrove, D.J. (2015). Plant cell wall extensibility: connecting plant cell growth with cell wall structure, mechanics, and the action of wall-modifying enzymes. Journal of Experimental Botany *67*, 463-476.

Cosgrove, D.J. (2018). Diffuse growth of plant cell walls. Plant Physiology *176*, 16-27.

Crowell, E.F., Bischoff, V., Desprez, T., Rolland, A., Stierhof, Y.-D., Schumacher, K., Gonneau, M., Höfte, H., and Vernhettes, S. (2009). Pausing of Golgi bodies on microtubules regulates secretion of cellulose synthase complexes in *Arabidopsis*. The Plant Cell *21*, 1141-1154.

Crowell, E.F., Timpano, H., Desprez, T., Franssen-Verheijen, T., Emons, A.-M., Höfte, H., and Vernhettes, S. (2011). Differential regulation of cellulose orientation at the inner and outer face of epidermal cells in the *Arabidopsis* hypocotyl. The Plant Cell *23*, 2592-2605.

Elsner, J., Lipowczan, M., and Kwiatkowska, D. (2018). Differential growth of pavement cells of Arabidopsis thaliana leaf epidermis as revealed by microbead labeling. American journal of botany *105*, 257-265.

Elsner, J., Michalski, M., and Kwiatkowska, D. (2012). Spatiotemporal variation of leaf epidermal cell growth: a quantitative analysis of *Arabidopsis thaliana* wild-type and triple cyclinD3 mutant plants. Annals of Botany *109*, 897-910.

Eng, R.C., and Sampathkumar, A. (2018). Getting into shape: the mechanics behind plant morphogenesis. Current Opinion in Plant Biology *46*, 25-31.

Fayant, P., Girlanda, O., Chebli, Y., Aubin, C.-É., Villemure, I., and Geitmann, A. (2010). Finite element model of polar growth in pollen tubes. The Plant Cell *22*, 2579-2593.

Fu, Y., Gu, Y., Zheng, Z., Wasteneys, G., and Yang, Z. (2005). *Arabidopsis* interdigitating cell growth requires two antagonistic pathways with opposing action on cell morphogenesis. Cell *120*, 687-700.

Fu, Y., Li, H., and Yang, Z. (2002). The ROP2 GTPase controls the formation of cortical fine F-actin and the early phase of directional

cell expansion during *Arabidopsis* organogenesis. The Plant Cell *14*, 777-794.

Fujita, M., Himmelspach, R., Ward, J., Whittington, A.T., Liu, C., Truong, T.T., Hasenbein, N., Galway, M.E., Mansfield, S.D., and Hocart, C.H. (2013). The any1 D604N mutation in the Arabidopsis thaliana cellulose synthase 1 catalytic domain reduces cell wall crystallinity and the velocity of cellulose synthase complexes. Plant physiology, pp. 112.211565.

Giannoutsou, E., Apostolakos, P., and Galatis, B. (2016). Spatio-temporal diversification of the cell wall matrix materials in the developing stomatal complexes of Zea mays. Planta *244*, 1125-1143.

Gu, Y., Kaplinsky, N., Bringmann, M., Cobb, A., Carroll, A., Sampathkumar, A., Baskin, T.I., Persson, S., and Somerville, C.R. (2010). Identification of a cellulose synthase-associated protein required for cellulose biosynthesis. Proceedings of the National Academy of Sciences of the United States of America *107*, 12866-12871.

Hamant, O., and Traas, J. (2010). The mechanics behind plant development. New Phytologist *185*, 369-385.

Han, B., Chen, L., Wang, J., Wu, Z., Yan, L., and Hou, S. (2015). Constitutive expresser of pathogenesis related genes 1 is required for pavement cell morphogenesis in *Arabidopsis*. PLoS One *10*, e0133249.

Ivakov, A., and Persson, S. (2013). Plant cell shape: modulators and measurements. Frontiers in Plant Science *4*, 439.

Jacques, E., Verbelen, J.-P., and Vissenberg, K. (2014). Review on shape formation in epidermal pavement cells of the *Arabidopsis* leaf. Functional Plant Biology *41*, 914-921.

Kirik, V., Herrmann, U., Parupalli, C., Sedbrook, J.C., Ehrhardt, D.W., and Hülskamp, M. (2007). CLASP localizes in two discrete patterns on cortical microtubules and is required for cell morphogenesis and cell division in *Arabidopsis*. Journal of Cell Science *120*, 4416-4425.

Korn, R.W. (1976). Concerning the sinuous shape of leaf epidermal cells. New Phytologist *77*, 153-161.

Korn, R.W., and Spalding, R.M. (1973). The geometry of plant epidermal cells. New Phytologist *72*, 1357-1365.

Kotzer, A., and Wasteneys, G. (2006). Mechanisms behind the puzzle: microtubule–microfilament cross-talk in pavement cell formation. Botany *84*, 594-603.

Landrein, B., and Hamant, O. (2013). How mechanical stress controls microtubule behavior and morphogenesis in plants: history, experiments and revisited theories. Plant Journal *75*, 324-338.

Le, J., Mallery, E.L., Zhang, C., Brankle, S., and Szymanski, D.B. (2006). *Arabidopsis* BRICK1/HSPC300 is an essential WAVE-complex subunit that selectively stabilizes the Arp2/3 activator SCAR2. Current Biology *16*, 895-901.

Liang, H., Zhang, Y., Martinez, P., Rasmussen, C., Xu, T., and Yang, Z. (2018). The microtubule-associated protein IQ67 DOMAIN5 modulates microtubule dynamics and pavement cell shape. Plant physiology, pp. 00558.02018.

Liesche, J., Ziomkiewicz, I., and Schulz, A. (2013). Super-resolution imaging with Pontamine Fast Scarlet 4BS enables direct visualization of cellulose orientation and cell connection architecture in onion epidermis cells. BMC plant biology *13*, 226.

Lin, D., Cao, L., Zhou, Z., Zhu, L., Ehrhardt, D., Yang, Z., and Fu, Y. (2013). Rho GTPase signaling activates microtubule severing to promote microtubule ordering in *Arabidopsis*. Current Biology *23*, 290-297.

Liu, X., Yang, Q., Wang, Y., Wang, L., Fu, Y., and Wang, X. (2018). Brassinosteroids regulate pavement cell growth by mediating BIN2-induced microtubule stabilization. Journal of Experimental Botany *69*, 1037-1049.

Majda, M., Grones, P., Sintorn, I.-M., Vain, T., Milani, P., Krupinski, P., Zagórska-Marek, B., Viotti, C., Jönsson, H., Mellerowicz, E.J.*, et al.* (2017). Mechanochemical polarization of contiguous cell walls shapes plant pavement cells. Developmental Cell *43*, 290-304.e294.

Marc, J., Granger, C.L., Brincat, J., Fisher, D.D., Kao, T.-h., McCubbin, A.G., and Cyr, R.J. (1998). A GFP–MAP4 reporter gene for visualizing cortical microtubule rearrangements in living epidermal cells. The Plant Cell *10*, 1927-1939.

Mathur, J. (2004). Cell shape development in plants. Trends Plant Sci *9*, 583-590.

Mathur, J. (2006). Local interactions shape plant cells. Current Opinion in Cell Biology *18*, 40-46.

Mathur, J., and Hülskamp, M. (2002). Microtubules and microfilaments in cell morphogenesis in higher plants. Current Biology *12*, R669-R676.

Mitra, D., Kumari, P., Quegwer, J., Klemm, S., Moeller, B., Poeschl, Y., Pflug, P., Stamm, G., Abel, S., and Bürstenbinder, K. (2018). Microtubule-associated protein IQ67 DOMAIN5 regulates interdigitation of leaf pavement cells in *Arabidopsis thaliana*. BioRxiv, 268466.

Möller, B., Poeschl, Y., Plötner, R., and Bürstenbinder, K. (2017). PaCeQuant: a tool for high-throughput quantification of pavement cell shape characteristics. Plant physiology, pp. 00961.02017.

Money, N. (2007). Biomechanics of invasive hyphal growth. In Biology of the fungal cell (Springer), pp. 237-249.

Mravec, J., Kračun, S.K., Rydahl, M.G., Westereng, B., Miart, F., Clausen, M.H., Fangel, J.U., Daugaard, M., Van Cutsem, P., and Henrik, H. (2014). Tracking developmentally regulated post-synthetic processing of homogalacturonan and chitin using reciprocal oligosaccharide probes. Development *141*, 4841-4850.

Murashige, T., and Skoog, F. (1962). A revised medium for rapid growth and bio assays with tobacco tissue cultures. Physiologia Plantarum *15*, 473-497.

Nakamura, M., Naoi, K., Shoji, T., and Hashimoto, T. (2004). Low concentrations of propyzamide and oryzalin alter microtubule dynamics in *Arabidopsis* epidermal cells. Plant and Cell Physiology *45*, 1330-1334.

Palin, R., and Geitmann, A. (2012). The role of pectin in plant morphogenesis. Biosystems *109*, 397-402.

Panteris, E., and Galatis, B. (2005). The morphogenesis of lobed plant cells in the mesophyll and epidermis: organization and distinct roles of cortical microtubules and actin filaments. New Phytologist *167*, 721-732.

Peaucelle, A., Wightman, R., and Höfte, H. (2015). The control of growth symmetry breaking in the *Arabidopsis* hypocotyl. Current Biology *25*, 1746-1752.

Peng, L., Xiang, F., Roberts, E., Kawagoe, Y., Greve, L.C., Kreuz, K., and Delmer, D.P. (2001). The experimental herbicide CGA 325′ 615 inhibits synthesis of crystalline cellulose and causes accumulation of non-crystalline β-1, 4-glucan associated with CesA protein. Plant Physiology *126*, 981-992.

Pezzulla, M., Smith, G.P., Nardinocchi, P., and Holmes, D.P. (2016). Geometry and mechanics of thin growing bilayers. Soft Matter *12*, 4435-4442.

Rosero, A., Oulehlová, D., Stillerová, L., Schiebertová, P., Grunt, M., Žárský, V., and Cvrčková, F. (2016). *Arabidopsis* FH1 formin affects cotyledon pavement cell shape by modulating cytoskeleton dynamics. Plant and Cell Physiology *57*, 488-504.

Rounds, C.M., Lubeck, E., Hepler, P.K., and Winship, L.J. (2011). Propidium iodide competes with Ca^{2+} to label pectin in pollen tubes and *Arabidopsis* root hairs. Plant Physiology *157*, 175-187.

Sampathkumar, A., Krupinski, P., Wightman, R., Milani, P., Berquand, A., Boudaoud, A., Hamant, O., Jönsson, H., and Meyerowitz, E.M. (2014). Subcellular and supracellular mechanical stress prescribes cytoskeleton behavior in *Arabidopsis* cotyledon pavement cells. ELife *3*, e01967.

Sapala, A., Runions, A., Routier-Kierzkowska, A.-L., Gupta, M.D., Hong, L., Hofhuis, H., Verger, S., Mosca, G., Li, C.-B., and Hay, A. (2018). Why plants make puzzle cells, and how their shape emerges. ELife *7*, e32794.

Schneider, C.A., Rasband, W.S., and Eliceiri, K.W. (2012). NIH Image to ImageJ: 25 years of image analysis. Nature Methods *9*, 671-675

Shaw, S.L., Dumais, J., and Long, S.R. (2000). Cell Surface Expansion in Polarly Growing Root Hairs ofMedicago truncatula. Plant Physiology *124*, 959-970.

Smith, L.G. (2003). Cytoskeletal control of plant cell shape: getting the fine points. Current Opinion in Plant Biology *6*, 63-73.

Smith, L.G., and Oppenheimer, D.G. (2005). Spatial control of cell expansion by the plant cytoskeleton. Annual Review of Cell and Developmental Biology *21*, 271-295.

Sotiriou, P., Giannoutsou, E., Panteris, E., Galatis, B., and Apostolakos, P. (2018). Local differentiation of cell wall matrix polysaccharides in sinuous pavement cells: its possible involvement in the flexibility of cell shape. Plant Biology *20*, 223-237.

Szymanski, D.B. (2014). The kinematics and mechanics of leaf expansion: new pieces to the *Arabidopsis* puzzle. Current Opinion in Plant Biology *22*, 141-148.

Torode, T.A., O'Neill, R.E., Marcus, S.E., Cornuault, V., Pose-Albacete, S., Lauder, R.P., Kracun, S.K., Rydahl, M.G., Andersen, M.C., and Willats, W.G.T. (2017). Branched pectic galactan in phloem-sieve-element cell walls: implications for cell mechanics. Plant physiology, pp. 01568.02017.

Uyttewaal, M., Burian, A., Alim, K., Landrein, B., Borowska-Wykręt, D., Dedieu, A., Peaucelle, A., Ludynia, M., Traas, J., and Boudaoud, A. (2012). Mechanical stress acts via katanin to amplify differences in growth rate between adjacent cells in *Arabidopsis*. Cell *149*, 439-451.

Vofely, R.V., Gallagher, J., Pisano, G.D., Bartlett, M., and Braybrook, S.A. (2018). Of puzzles and pavements: a quantitative exploration of leaf epidermal cell shape. bioRxiv.

Watson, R. (1942). The effect of cuticular hardening on the form of epidermal cells. New Phytologist, 223-229.

Wolf, S., Mouille, G., and Pelloux, J. (2009). Homogalacturonan methyl-esterification and plant development. Molecular Plant *2*, 851-860.

Wu, Y., Zhao, S., Tian, H., He, Y., Xiong, W., Guo, L., and Wu, Y. (2013). CPK3-phosphorylated RhoGDI1 is essential in the development of *Arabidopsis* seedlings and leaf epidermal cells. Journal of Experimental Botany *64*, 3327-3338.

Xu, T., Wen, M., Nagawa, S., Fu, Y., Chen, J.-G., Wu, M.-J., Perrot-Rechenmann, C., Friml, J., Jones, A.M., and Yang, Z. (2010). Cell surface-and rho GTPase-based auxin signaling controls cellular interdigitation in *Arabidopsis*. Cell *143*, 99-110.

Yanagisawa, M., Desyatova, A.S., Belteton, S.A., Mallery, E.L., Turner, J.A., and Szymanski, D.B. (2015). Patterning mechanisms of cytoskeletal and cell wall systems during leaf trichome morphogenesis. Nature Plants *1*, 15014.

Zhang, C., Halsey, L.E., and Szymanski, D.B. (2011). The development and geometry of shape change in *Arabidopsis thaliana* cotyledon pavement cells. BMC plant biology *11*, 1-13.

Supplemental Movies

Movie S1. 3D reconstruction of confocal z-stack demonstrating pavement cells of *Arabidopsis* cotyledon stained with PFS for cellulose. Locations of necks (indentations) on periclinal walls are clearly associated with a markedly higher signal. Related to Figs. S5D and E.

Movie S2. 3D reconstruction of confocal z-stack demonstrating pavement cells of *Arabidopsis* cotyledon stained with calcofluor white for cellulose. Locations of necks (indentations) on periclinal walls are clearly associated with a markedly higher signal. The cellulose enriched zones are present on both anticlinal and periclinal walls. Related to Figs. 6D, L and S5F.

Movie S3. 3D reconstruction of confocal z-stack demonstrating microtubules in pavement cells of *Arabidopsis* cotyledon from GFP-TUB6 line. Microtubules are enriched on neck sides while comparatively scarce on the lobe sides of the anticlinal walls. These microtubules seem to be continuous between periclinal and anticlinal walls. Related to Fig. 6B and C.

Movie S4. 3D reconstruction of confocal z-stack demonstrating microtubules (orange, GFP-MAP4) and cell wall (green, propidium iodide) in pavement cells of *Arabidopsis* cotyledon. Marking the cell borders with the green channel (appears and disappears during the movie) reveals that microtubules are enriched on the neck sides. Related to Figs. 6A.

Movie S5. 3D reconstruction of confocal z-stack demonstrating microtubules in pavement cells of *Arabidopsis* cotyledon from GFP-TUB6 line. Arrows show microtubules extending between the periclinal and anticlinal walls at neck locations of tiny bends formed in the cell wall. Related to Figs. 6B and C.

Supplemental Information

Available in the online version.